

**CASE FILE
COPY**

**PERFORMANCE OPTIMIZED,
SMALL STRUCTURALLY INTEGRATED
ION THRUSTER SYSTEM**

J. HYMAN, JR.

**HUGHES RESEARCH LABORATORIES
A DIVISION OF HUGHES AIRCRAFT COMPANY
3011 MALIBU CANYON ROAD
MALIBU, CALIFORNIA 90265**

**PREPARED FOR
NATIONAL AERONAUTICS AND SPACE ADMINISTRATION
NASA LEWIS RESEARCH CENTER
CLEVELAND, OHIO 44135**

CONTRACT NAS 3-15483

NOTICE

This report was prepared as an account of Government-sponsored work. Neither the United States, nor the National Aeronautics and Space Administration (NASA), nor any person acting on behalf of NASA:

- A.) Makes any warranty or representation, expressed or implied, with respect to the accuracy, completeness, or usefulness of the information contained in this report, or that the use of any information, apparatus, method, or process disclosed in this report may not infringe privately-owned rights; or
- B.) Assumes any liabilities with respect to the use of, or for damages resulting from the use of, any information, apparatus, method or process disclosed in this report.

As used above, "person acting on behalf of NASA" includes any employee or contractor of NASA, or employee of such contractor, to the extent that such employee or contractor of NASA or employee of such contractor prepares, disseminates, or provides access to any information pursuant to his employment or contract with NASA, or his employment with such contractor.

Requests for copies of this report should be referred to

National Aeronautics and Space Administration
Scientific and Technical Information Facility
P.O. Box 33
College Park, Md. 20740

1. Report No. CR-121183	2. Government Accession No.	3. Recipient's Catalog No.	
4. Title and Subtitle PERFORMANCE OPTIMIZED, SMALL STRUCTURALLY INTEGRATED ION THRUSTER SYSTEM		5. Report Date May 1973	6. Performing Organization Code
		8. Performing Organization Report No.	
7. Author(s) Julius Hyman, Jr., (See Program Participation Page)		10. Work Unit No.	
9. Performing Organization Name and Address Hughes Research Laboratories 3011 Malibu Canyon Road Malibu, California 90265		11. Contract or Grant No. NAS 3-15483	
		13. Type of Report and Period Covered Contractor Report	
12. Sponsoring Agency Name and Address National Aeronautics and Space Administration Washington, D. C. 20546		14. Sponsoring Agency Code	
		15. Supplementary Notes	
16. Abstract <p>A 5-cm Structurally Integrated ion Thruster has been developed for attitude control and stationkeeping of synchronous satellites. As optimized with a conventional ion extraction system, the system demonstrates a thrust $T = 0.47$ mlb at a beam voltage $V_B = 1600$ V ($I_{sp} = 3040$ sec), total mass efficiency $\eta_m = 76\%$, and electrical efficiency $\eta_E = 56\%$. Under the subject contract effort, no significant performance change was noted for operation with ($\pm 10^\circ$) two dimensional electrostatic thrust-vectoring grids. Structural integrity with the vectoring grids was demonstrated for shock (± 30 G), sinusoidal (9 G), and random (19.9 G rms) accelerations. System envelope is 31.2 cm long by 13.4 cm flange bolt circle, with a mass of 9.0 Kg, including 6.8 Kg mercury propellant.</p>			
17. Key Words (Suggested by Author(s)) Mercury Propellant Electron Bombardment Ion Propulsion System Vibration Test Performance Test 5 cm Diameter		18. Distribution Statement Unclassified - Unlimited	
19. Security Classif. (of this report) Unclassified	20. Security Classif. (of this page) Unclassified	21. No. of Pages 86	22. Price* 3.00

PROGRAM PARTICIPATION

Contributions by members of the HRL technical staff who participated in the program are acknowledged below.

PROGRAM MANAGEMENT	J. Hyman, Jr.
DESIGN	S. Kami P. Francisco
DYNAMIC ANALYSIS	H.H. Cooley, Jr.
STRESS ANALYSIS	J.K. Lippit and J.S. Quiaoit
STRUCTURAL TESTING	A.J. Petersen R.D. McKain
THRUSTER TESTING	C.R. Dulgeroff

TABLE OF CONTENTS

	LIST OF ILLUSTRATIONS	vii
	ABSTRACT	ix
I	INTRODUCTION	1
II	TECHNICAL PROGRAM	5
	A. The SIT-5 Ion Propulsion System: (A Summary)	5
	B. System Optimization	22
	C. Performance Optimization	23
	D. Test Qualifications	40
	E. Areas for Continued Development	79
III	SUMMARY OF RESULTS	83
	REFERENCES	85

LIST OF ILLUSTRATIONS

Fig. 1.	First generation SIT-5 system	2
Fig. 2.	Structurally integrated thruster	6
Fig. 3.	Deflection angle versus x-deflection voltage	10
Fig. 4.	Deflection angle versus y-deflection voltage	11
Fig. 5.	SIT-5 ion thruster	15
Fig. 6.	SIT-5 thruster components	16
Fig. 7.	Discharge chamber with main-cathode subassembly attached	21
Fig. 8.	Analysis flow chart for SIT-5 redesign	30
Fig. 9.	Neutralizer-vaporizer (NV) subassembly with integral enclosed keeper electrode	34
Fig. 10.	SIT-5 CIV subassembly with swaged metal to insulator connection	36
Fig. 11.	(a) Hughes hollow cathode subassembly	37
Fig. 11.	(b) SIT-5 cathode with plasma spray alumina encapsulated heater element	37
Fig. 12.	Engineering drawing of SIT-5 CIV	39
Fig. 13.	S/N thruster showing fracture of two ceramic support insulators	42
Fig. 14.	Redesigned thruster support insulators	43
Fig. 15.	S/N 201 thruster showing loss of optics sputter shield and fracture of solid- nickel lead wire	46
Fig. 16.	Metal crescent which broke loose from the foot of a magnetic retainer clamp	46
Fig. 17.	Ground screen of S/N 202 thruster showing material shredding and the loss of a small piece of screen	48

Fig. 18.	Thrust vector optics S/N 601 after vibration test on SIT-5 thruster S/N 201	50
Fig. 19.	Neutralizer position during performance mapping of S/N 201 module	58
Fig. 20.	Neutralizer-keeper current versus neutralizer-keeper voltage	59
Fig. 21.	Neutralizer flowrate equivalent versus neutralizer keeper voltage	61
Fig. 22.	Main keeper current versus main keeper voltage, discharge chamber voltage, discharge chamber current, and beam current	62
Fig. 23.	Main cathode flowrate versus discharge chamber voltage, discharge chamber current and beam current	63
Fig. 24.	Perveance curves for SIT-5	65
Fig. 25.	Discharge chamber current as a function of cycle test	71
Fig. 26.	Eight channel recorder data for accelerated cycle test	75
Fig. 27.	Baffle and baffle support after duty cycle test	79
Fig. 28.	Main vaporizer heater defect	80

ABSTRACT

A 5-cm Structurally Integrated ion Thruster has been developed for attitude control and stationkeeping of synchronous satellites. As optimized with a conventional ion extraction system, the system demonstrates a thrust $T = 0.47$ mlb at a beam voltage $V_B = 1600$ V ($I_{sp} = 3040$ sec), total mass efficiency $\eta_m = 76\%$, and electrical efficiency $\eta_E = 56\%$. Under the subject contract effort no performance change was noted for operation with ($\pm 10^\circ$) two dimensional electrostatic thrust-vectoring grids. Structural integrity with the vectoring grids was demonstrated for shock (± 30 G), sinusoidal (9G), and random (19.9 G rms) accelerations. System envelope is 31.2 cm long by 13.4 cm flange bolt circle, with a mass of 9.0 Kg, including 6.8 Kg mercury propellant.

SECTION I

INTRODUCTION

There is an increasing need of low thrust (~ 1 mlb) propulsion devices for attitude control and stationkeeping of synchronous satellites. As the technology of electron bombardment thrusters advances along with associated development of solar cells and power conditioning equipment, it becomes apparent that these systems will find space application in the near future.

Under Contract NAS 3-14129, Hughes Aircraft Company has analyzed, designed, fabricated and tested a first generation SIT-5 thruster system¹ (see Fig. 1) which is suitable for attitude control and stationkeeping of a synchronous satellite. When paired with the thrust-vectorable ($\pm 10^\circ$) ion-extraction system (developed under NASA contract NAS 3-14058) the system provides 0.56 mlb of thrust with a net accelerating voltage of 1200 V with a propellant utilization efficiency of 64% (including neutralizer losses), and a system electrical efficiency of 47%. The mass of the system is 8.5 Kg including the propellant mass of 6.2 Kg. Structural integrity of the first-generation SIT-5 system has been proven by a series of shock and vibration tests.

The present program has offered an opportunity to advance knowledge gained from the earlier effort in development of a second-generation 5-cm thruster system. The program has included structural and performance optimization, followed by qualification and durability testing. The goal of this program has been to advance the performance level of the SIT-5 system to the following minimum standards:

- a. Performance standards:
 - (1) Startup to design-performance operation within a minimum time not to exceed thirty (30) minutes
 - (2) Operating characteristics which permit stable closed-loop control operation

M 7635



Fig. 1. First generation SIT-5 system (the thruster is shown here with dielectric-coated optics).

(3) Thrust vector angle, ± 10 degrees variable continuously

(4) Projected Lifetime, 10,000 hours.

b. Performance parameters:

(1) Electrical efficiency, $\eta_E = 0.50$ or higher

(2) Propellant utilization efficiency, $\eta_m = 0.76$
(including neutralizer losses)

(3) Overall efficiency, $\eta_T = 0.36$ or higher

(4) Specific impulse, $I_{sp} = 3040$ sec,
approximately

(5) Net accelerating voltage, $V_B = 1600$ V

(6) Thrust, $T = 0.46$ mlb

(7) Approximate total mass, 2.1 Kg or less
(not including mercury propellant).

Page Intentionally Left Blank

SECTION II

TECHNICAL PROGRAM

A technical program is described below in which development of the SIT-5 ion propulsion system was advanced from the level achieved under an earlier NASA Contract (NAS 3-14129). The second generation device includes an ion extraction system (developed under NASA Contract NAS 3-15385) having a capability for two-dimensional electrostatic ion beam deflection.² A photograph of the SIT-5 system is shown in Fig. 2, complete with the thrust-vectoring extraction system. In the discussion which follows, system characteristics are described in detail with respect to steady state and cyclic operation (including the thrust vectoring capability), and with respect to its structural integrity to withstand the booster-launch environment. Optimization of system performance and structural design are also discussed and specific techniques and accomplishments are identified. At the conclusion of this discussion, specific tests are described which provide the basis for space qualification of system performance.

A. THE SIT-5 ION PROPULSION SYSTEM (A SUMMARY)

A 5-cm Structurally integrated Ion Thruster (SIT-5) has been flight qualified under the subject NASA contract to the levels indicated in Table I. This system makes use of the technology established by NASA in development of the SERT II ion propulsion system³ and extends it to a range of thrust level which is suitable for attitude control and stationkeeping of a synchronous satellite.

M8494

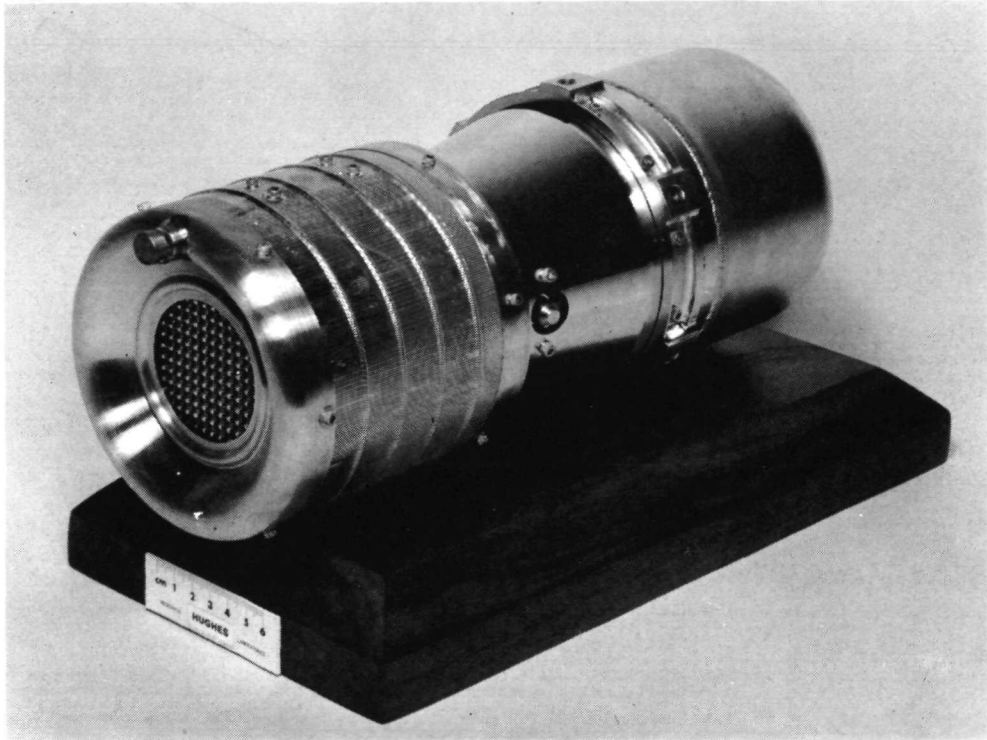


Fig. 2. Structurally integrated thruster (SIT-5) developed under NASA Contract NAS 3-15385.

TABLE I

SIT-5 System Qualifications

Parameter	Value
<u>Thruster Operating Characteristics</u>	
Thrust, T, mlb	0.47
Specific Impulse, I_{sp} , sec	3040.00
Power Requirements, P_T , W	72.20
Electrical Efficiency, η_E , %	56.00
Propellant Utilization, including neutralizer losses, η_m , %	76.00
Overall efficiency, η_T , %	43.00
<u>Beam Deflection</u> (in two-dimensions)	$\pm 10^\circ$
<u>Cyclic Operation</u>	
Power-off to beam-on period, τ_{cyclic} , min	30.00
Cyclic capability, N_{cyclic}	$\sim 1,000.00$
<u>Mass</u>	
Mass excluding propellant, kg	2.20
Mass including 6.8 kg of propellant, kg (sufficient for 30,000 hours full beam operation)	9.00
<u>Size</u>	
Length, cm	31.20
Diameter, cm	12.10
Mounting flange, diameter, cm	13.40
<u>Structural Qualifications (each Axis)</u>	
Sinusoidal, G	9.00
Random, G rms	19.90
Shock, G	± 30.00

T925

1. Thruster Operating Characteristics

The capabilities of thruster performance were established by a comprehensive program of discharge chamber optimization. For purposes of the optimization, a conventional ion extraction system was employed to represent the vectorable design which was then under concurrent development. As shown in Table II, the optimized system provides design thrust $T = 0.47$ mlb at a net accelerating voltage $V_B = 1600$ V with a propellant utilization efficiency $\eta_m = 76\%$ (including neutralizer losses), and a system electrical efficiency $\eta_E = 56\%$.

Following the research studies of Hall, et al.,⁴ and Nakanishi, et al.,⁵ an enclosed keeper geometry was chosen for use in the SIT-5 system both for the main discharge and neutralizer cathode application. The vapor flow impedance afforded by the enclosed keeper configuration has permitted satisfactory neutralizer coupling with the ion beam to be achieved with neutralizer vapor flowrates as low as 1.0 mA equivalent. The neutralizer cathode is located so that the aperture of the neutralizer-keeper electrode is placed at a position 2.71 cm downstream and 2.71 cm radially outward from the outermost beam aperture of the ion extraction system. The axis of the neutralizer is directed straight downstream parallel to the thruster axis.

The system was operated with the electrostatic vectoring grids only after the system was combined with its flight-type propellant feed system. In this configuration, electrical performance was virtually unchanged, and no significant change in mass utilization efficiency was detectable from thruster mass measurements conducted before and after that operation.* Deflections of $\pm 10^\circ$ were attained repeatably in the X and Y directions (orthogonal to the thrust direction) with accelerating currents remaining relatively constant at 0.08 mA. The thrust vectoring data are summarized in Figs. 3 and 4.

*For operation of the same SIT-5 thruster with the electrostatic vectoring system under NASA Contract NAS 3-15385, on the other hand, a significant decrease in propellant utilization was reported for measurements with a burrette feed system.² This discrepancy has not been resolved under the contract effort.

TABLE II

SIT-5 System Performance Profile (For Operation at the Design Set Point of Contract NAS 3-15483)

Nominal Operating Parameters	Operating Values (Test 102-TV-9)
Beam Voltage [*] , V	1600
Beam Current, mA	25.6
Accel Voltage [*] , V	-800
Accel Drain Current, mA (at 0° deflection)	0.075
Discharge Voltage, V	45
Discharge Current, mA	260
Discharge Power, W	11.7
Cathode	
Keeper Voltage, V	18
Keeper Current, mA	365
Keeper Power, W	6.6
Heater Power, W	0
Vaporizer Voltage, V	3.2
Vaporizer Current, A	1.3
Vaporizer Heater Power, W	4.2
Neutralizer	
Keeper Voltage, V	17
Keeper Current, mA	365
Keeper Power, W	6.2
Heater Power, W	0
Vaporizer Voltage, V	2.3
Vaporizer Current, A	1
Vaporizer Heater Power, W	2.3
Coupling Voltage, V	11
Output Beam Power, W	40.3
Total Input Power, W	72.2
Thruster Propellant Flow	31.1
Equivalent, mA (cathode flow)	
Neutralizer Propellant Flow Equivalent, mA	2.6
Propellant Utilization Efficiency (including neutralizer), %	76
Electrical Efficiency, %	56
Over-all Efficiency, %	43
Discharge Loss, eV/ion	465
Thrust, mlb	0.47
Specific Impulse, sec	3040
Power-to-Thrust Ratio, W/mlb	154

* For experimental convenience, data for test 102-TV-9 were actually generated at a beam and accel voltage of 1200 V each rather than the design point values listed above. Subsequent operation of the SIT-5 system at the design point demonstrates that no significant error was introduced by this expedient.

T452

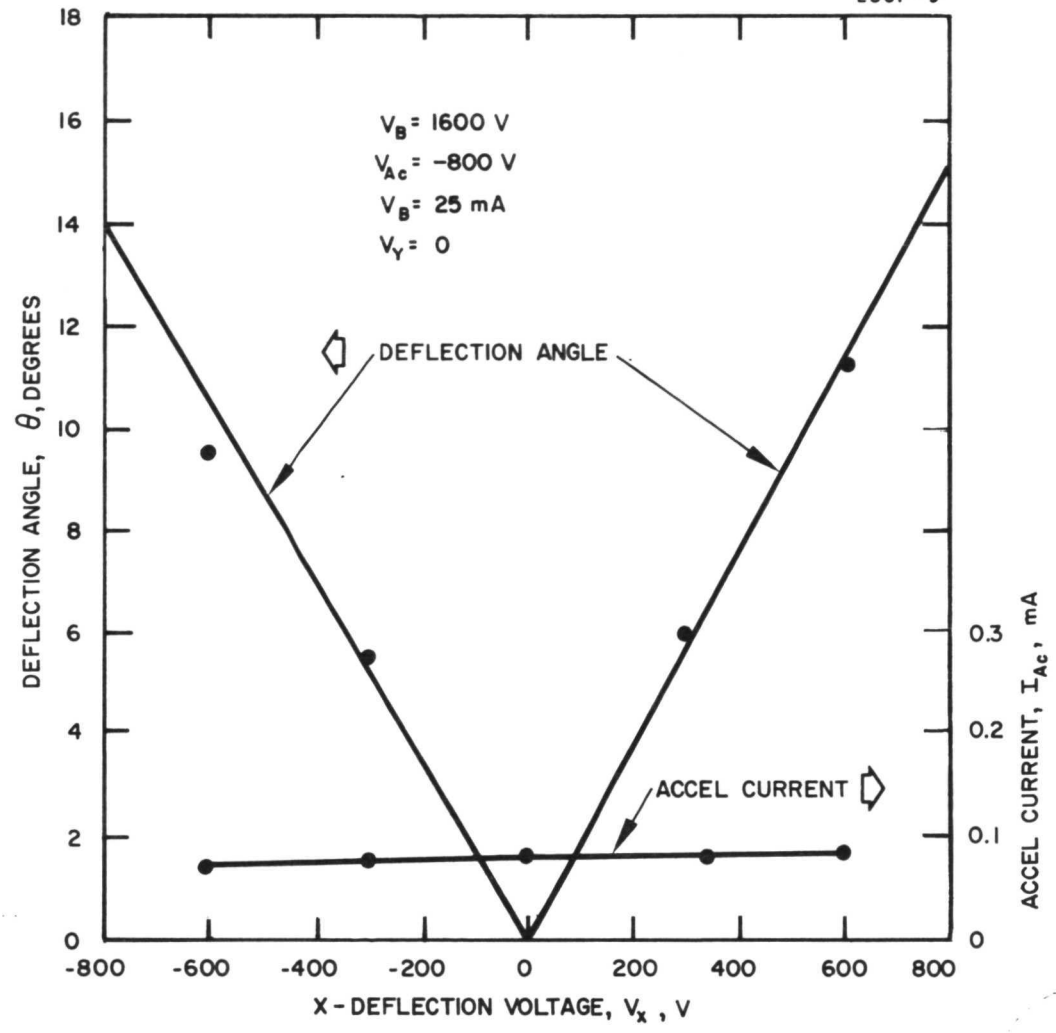


Fig. 3. Deflection angle versus x-deflection voltage.

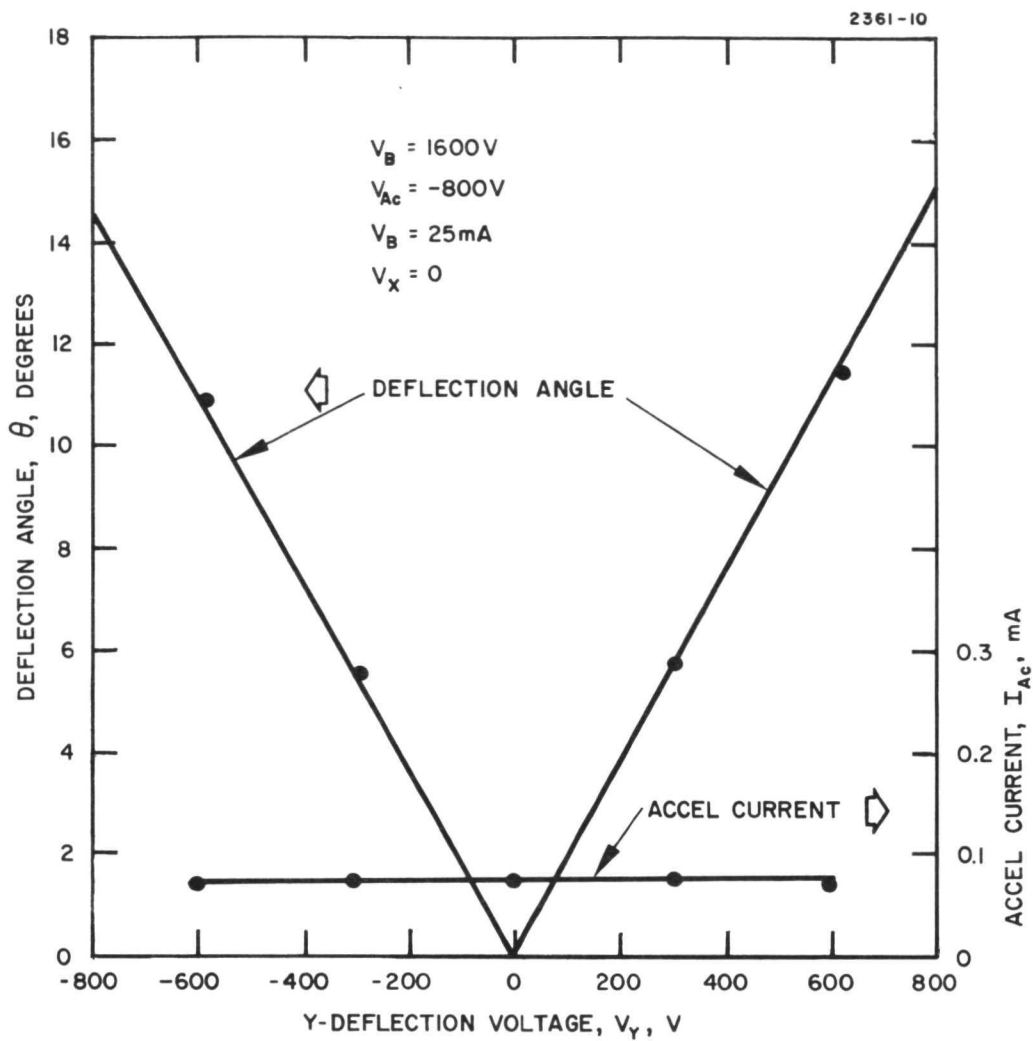


Fig. 4. Deflection angle versus y-deflection voltage.

Figures 3 and 4 show that X- and Y- deflections up to $\pm 10^\circ$ can be attained with a deflection voltage between ± 600 V. Because of the asymmetries in the interlocking electrode structures, the Y- deflection electrodes produce a larger deflection for an equivalent voltage than the X-electrodes. It can also be seen in Figs. 3 and 4 that the accel current is nearly constant over the deflection ranges of $\pm 10^\circ$. Although the data presented are for X- and Y-axis deflection only, combinations of these orthogonal deflections combine linearly to produce any off-axis deflection.

No extended lifetime demonstration was carried out under the contract effort, because that demonstration was scheduled for execution at the Lewis Research Center as part of the in-house NASA effort.⁶ As of October 1972, the SIT-5 had been operated under that effort for over 8,000 hours.⁷

The longest continuous operation under the contract effort was carried out at HRL in conjunction with a scheduled 165-hour Durability Test and another 116 hours of operation prior to Performance Mapping. No variation in thruster performance or thrust vectoring characteristics was detected over that period. At the conclusion of the Durability Test, thruster performance was mapped as a function of systematic variations of each significant operating parameter about the set point for nominal operation. The nominal set point was shown to represent an optimal operating condition, and operation throughout the variation was stable and repeatable.

A demonstration of cyclic operation was also carried out under the contract effort. In the Duty Cycle Test, the thruster was cycled from the power-off to the full beam-on condition repetitively over various periods to establish its capability to function in the mode anticipated for North-South stationkeeping of a synchronous satellite. In a final 500-hour Accelerated Duty Cycle Test, the thruster was cycled every 30 minutes to establish its capability for a lifetime in excess of 1000 cycles.

2. Structural Qualification

The structural integrity of the basic SIT-5 system has been demonstrated under the subject contract by a series of shock and vibration tests. This system satisfied design expectations with only minor exceptions which have now been corrected by straightforward component design modifications. The tested SIT-5 system included the electron-bombardment mercury ion thruster, a main cathode-isolator-vaporizer (CIV) subassembly, a neutralizer vaporizer (NV) subassembly, and a gas-pressurized propellant reservoir containing 6.8 kG of liquid mercury. The system was subjected to shock, sinusoidal, and random accelerations in each of the three mutually perpendicular axes in order to simulate the conditions encountered during rocket launching.

a. Shock Tests

In these tests, the SIT-5 system was subjected to three half-sine pulses in the positive and negative directions along each of the primary axes. The pulse amplitude was 30 G and the duration was 8 msec. The applied shock pulses were monitored by means of an accelerometer which had a resonant frequency of approximately 20 kHz.

b. Sinusoidal Vibration Tests

The system was also subjected to sinusoidal vibration along the three primary axes at levels defined in Table III below.

TABLE III
Sinusoidal Vibration Test Levels

Frequency	Level
5 - 19 Hz	0.5 in. double amplitude
19 - 2000 Hz	9 G's (0-peak)
Sweep Rate: 2 octaves/min.	

T176

c. Random Vibration Tests

The SIT-5 system was subjected to random vibrations along each axis at levels defined in Table IV.

TABLE IV
Random Vibration Test Levels

Frequency Band	Power Spectral Density
20 - 340 Hz	0.11 G ² /Hz
340 - 400 Hz	Up 12 dB/octave
400 - 2000 Hz	0.22 G ² /Hz
Over-all Level: 19.9 G rms Duration: 5.4 min/axis	

T454

3. System Design and Fabrication

An isometric drawing of the SIT-5 system is shown in Fig. 5. A photograph of separate components of the thruster system is shown in Fig. 6. The mercury propellant reservoir is fabricated by welding thin hemispherical shells (10 cm in diameter) to separate flanges which are grooved on the mating faces to accept a sealing ring of the butyl rubber bladder. The circular cross section of the sealing ring is molded as an integral part of the bladder edge. The hemispherical shell, which is upstream of the reservoir assembly, is perforated to allow passage of the pressurizing nitrogen gas to drive the mercury supply to the main and neutralizer cathodes. The gas reservoir is fabricated from a thin stainless steel plate which is drawn into a cylindrical shell and welded to an extension of the system mounting flange. To increase its pressure-holding capability, the upstream end of the gas reservoir is formed to a concave radius. The gas

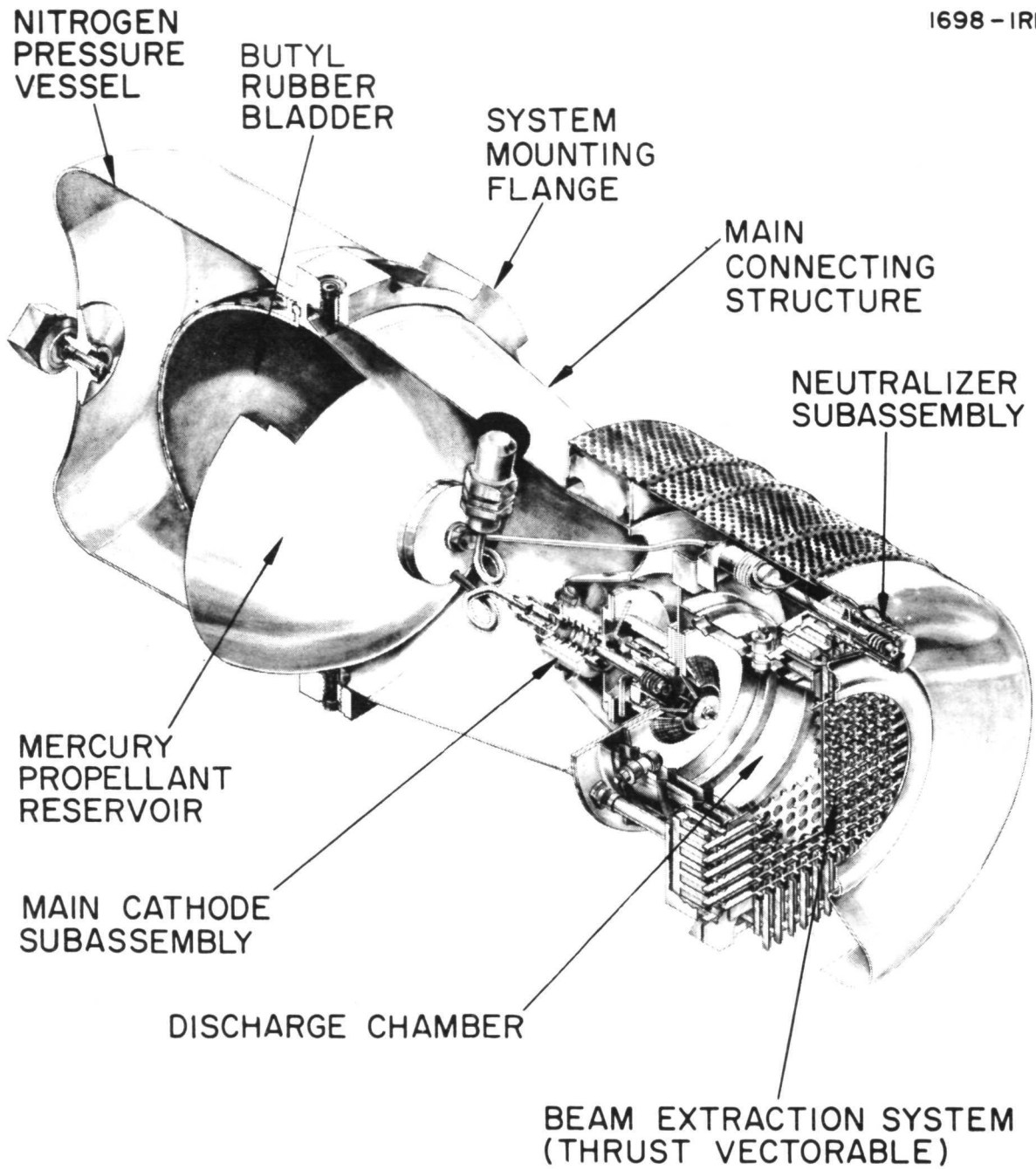


Fig. 5. SIT-5 ion thruster.

M8516



Fig. 6. SIT-5 thruster components.

reservoir is equipped with a gas fill valve of the type commonly used in aircraft medium-pressure gas storage tanks. This valve is needed only for temporary service prior to installation of a stainless steel valve-stem cover which seals the gas reservoir with a rubber O-ring. The downstream end of the propellant reservoir is fitted with a stainless steel manifold with rubber O-rings providing the required seals for connecting propellant lines from a propellant fill valve and to the main and neutralizer cathodes.

The downstream hemisphere of the propellant reservoir is welded directly to an extension of the system mounting flange. The perforated hemisphere, on the other hand, is pressed against the flange by means of a large diameter retainer ring which is threaded directly onto the system mounting flange. After the bladder O-ring is fully compressed by the rotation of the retainer ring, the ring is tack welded to the flange to prevent possible rotation as a result of vibration during booster launch. This design benefits from the fact that compression of the O-ring seal is brought about by structural members which are stressed in compression and tension with minimal moment for tearing or bending strains.

The thruster is attached to four support insulators which are brazed to a thruster support structure. Prior to final assembly, this structure is temporarily supported from the system mounting flange by four preassembly mounting tabs. This permits final connection of all propellant feed lines prior to enclosing the attachment region with the main connecting structure (which provides structural connection of the thruster support structure with the system mounting flange).

The downstream end of the main connecting structure is formed to provide an enclosed mounting surface for electrical connections. Support of the ground screen and front shield, and partial support point for the neutralizer support bracket is also provided.

The neutralizer cathode and vaporizer assembly is supported by a thin-walled bracket which projects from the downstream end of the connecting structure and is attached to the ground screen shield.

Appropriate thermal design insures that no condensation of the mercury vapor occurs in the region between the vaporizer and the cathode.

The thruster endplate (formed from mild steel) is attached to the four support insulators which are brazed to the support shell structure. The baffle and the cathode pole piece assembly are bolted (with lock-nuts) to the inside face of the thruster endplate.

The thruster outer shell is fabricated by rolling thin stainless steel sheet stock to a cylindrical shape 6.4 cm in diameter by 4.8 cm long; a seamless junction is formed by electron-beam welding. The thruster shell is spot welded to iron rings at either end which interface with the iron endplate and the ion extraction system, respectively. The anode is formed and beam-welded in a similar manner and attached to the thruster outer shell by insulator assemblies. To strengthen the structures stiffening ribs are rolled into the thruster and anode shells.

A complete mass breakdown of the SIT-5 system is given in Table V.

The main cathode design employs a 0.32 cm diameter enclosed hollow cathode. The cathode is integrated with the vaporizer and isolator to form a CIV subassembly. This assembly is mounted with a detachable flange to the isolator support shell, and the mercury feed tube is mated with the reservoir through a detachable connector as described previously. A strain-relief loop is formed in the feed line between the reservoir and the main vaporizer to reduce stresses which might result from relative motion between these components during launch. The neutralizer cathode is a 0.32 cm enclosed hollow cathode with integrally welded 0.69 cm vaporizer and associated tubulation which constitutes the NV subassembly. The mercury feed line of the neutralizer assembly is also attached with a detachable connector to the propellant reservoir. The neutralizer, main cathode, and vaporizer housings are fabricated from seamless thin wall tantalum tubing.

A unique design feature is incorporated into the main and neutralizer vaporizers to prevent liquid mercury from being driven through the pores of the vaporizer plug by the high dynamic pressures generated

TABLE V

Mass Breakdown of the SIT-5 System

System Component	Component Mass, grams
Thruster (including TV optics shell, anode, magnets and magnetics)	244.5
Electron Baffle	18.0
Thruster Endplate (with cathode pole piece)	39.1
Reservoir Vessels (with preassembly support tabs, isolator-support cone, pressure transducer, fill valve and cap, gas valve and cap, mounting flange, and leads to pressure transducer and thermocouple)	1299.9
Main Connecting Structure (with insulating terminals)	361.3
NV Assembly (with keeper and mounting bracket)	61.0
Ground Screen and Mask	61.3
CIV Subassembly with Keeper	89.7
Fastenings	<u>15.0</u>
Mass of Thruster Without Propellant	2189.8
Mass of Propellant	<u>6800.0</u>
Mass of Thruster With Propellant	8989.8

T927

during booster launch into earth orbit. Under the maximum shock loading of 30 G anticipated by the predesign analysis, a total hydrostatic pressure of 110 N/cm^2 is generated at the neutralizer location which tends to cause mercury intrusion through the $1.8 \mu\text{m}$ pores of the vaporizer plug. To prevent such intrusion, a 0.65-cm high porous tungsten column is enclosed inside both of the mercury feedlines, upstream of the vaporizer disk as shown in Fig. 7. This column acts as a surge volume to absorb the total quantity of inertia-limited mercury flow which passes through the feed lines during the shock loadings anticipated in the design analysis. At a total hydrostatic pressure of 28 N/cm^2 , the flow begins to penetrate the $4.5 \mu\text{m}$ diameter pores of the tungsten column, and this serves to limit the pressure below the value that would cause intrusion into the vaporizer plug. A channel is provided through the axis of the column to permit free transmission of mercury liquid to the vaporizer plug during normal operation. This opening does not compromise the pressure-limiting feature, since the necessary flow constriction occurs at the feed.

Figure 7 shows, in detail, the manner in which the main-cathode subassembly and discharge chamber are supported by a conical element which attaches directly to the main connecting structure. The alumina isolator body and all alumina thruster-support insulators are held in compression during assembly and under peak-load conditions; this increases the strength of the ceramic supports by an order of magnitude. The four thruster-support insulators are placed in compression by pressing them (by means of central stainless-steel lugs) against a second set of four insulators which are inserted from the opposite side of Kovar bushings. With all four thruster support insulators placed in compression by this expedient, it is possible (in the final assembly) to ensure that the isolator ceramic is also placed in compression without placing the support insulators in tension.

A magnetic field is generated inside the discharge chamber by permanent magnets which span the gap from the discharge-chamber end-plate to the collar polepiece. As indicated in Fig. 7 the field is

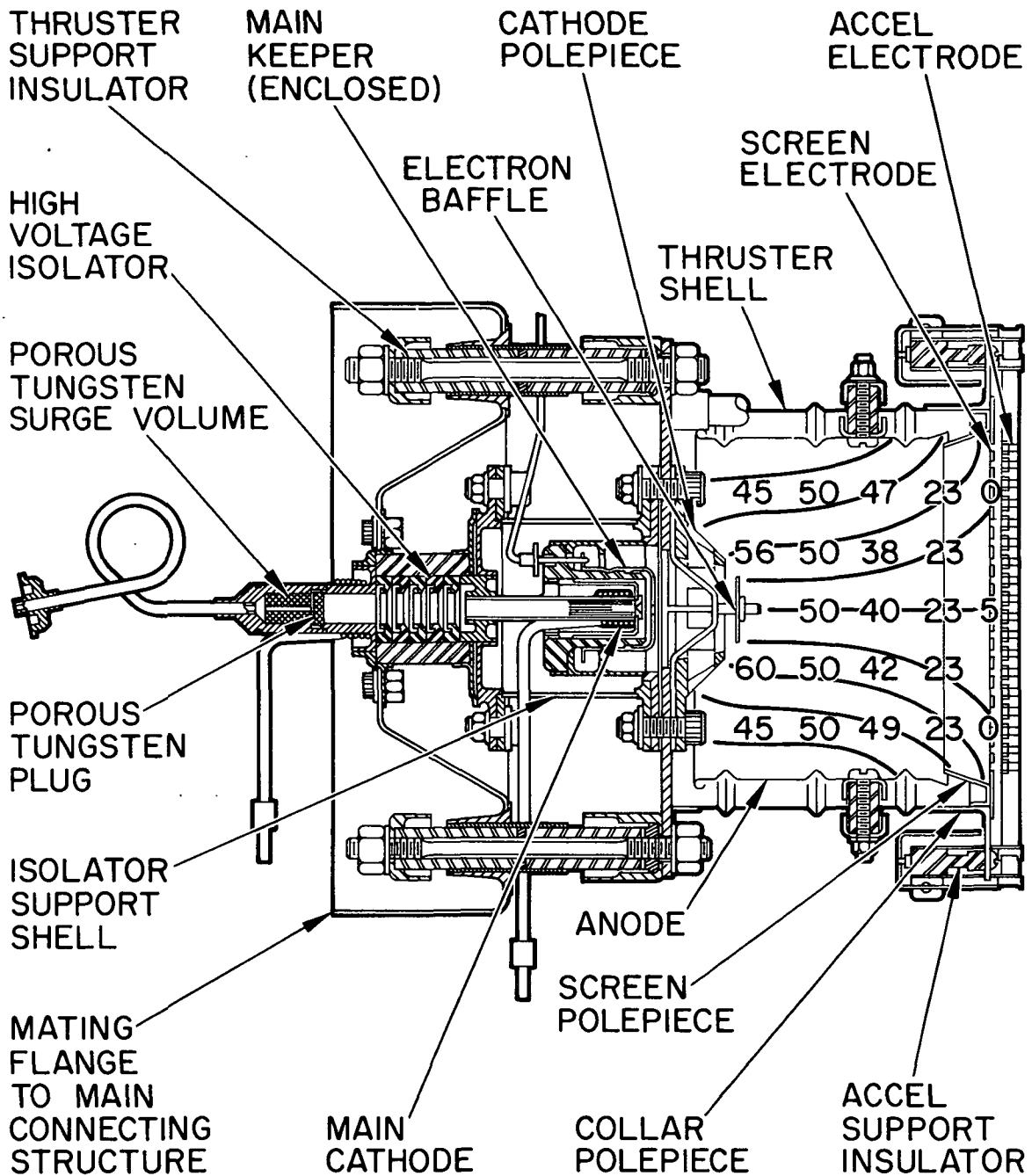


Fig. 7. Discharge chamber with main-cathode subassembly attached. The magnetic field shape is shown with values of the axial field component indicated in Gauss.

directed axially for the most part, but diverges at the downstream end in a manner determined by the shape of screen and cathode polepieces. All elements of the magnetic circuit are fabricated of type 1018 mild steel. General aspects of this magnetic design are typical of all ion thrusters which are adapted from the SERT II configuration.

The beam-extraction system provides an electrostatic thrust-vectoring capability of 10° from the thruster axis in any azimuthal direction. Individual beam deflection elements consist of thin, flat molybdenum electrodes which are slotted to form an interlocking structure which functions as the accel electrode. A conventionally drilled molybdenum plate serves as the screen electrode. The accel elements are supported at each end by fingers extending from four molybdenum spring-tension strips which are brazed to long rectangular accel-support insulators which are bolted to each edge of a rectangular extension of the collar polepiece. Small pins brazed to the ends of the accel elements lock into recesses provided on the bent tab of the spring fingers. The 89 circular beam forming apertures of the screen electrode are each 0.317 cm in diameter and are arranged in a square pattern with a 0.445-cm center-to-center spacing. This provides a screen open-area to total-area ratio of 36%. The individual beam-deflection elements are each 0.254-cm high and separated so as to form an array of square apertures which are 0.266 cm on a side.

B. SYSTEM OPTIMIZATION

At the onset of the subject contract, an effort was initiated to re-examine the first-generation SIT-5 system (developed under Contract NAS 3-14129) in order to identify areas of performance optimization and structural design where technical advancements would significantly enhance system acceptability. Building upon the experience gained in assembly and testing of the earlier configuration, it has been possible to streamline the steps required for final assembly and disassembly, and (by design) to insure accurate registration of

critical dimensions. A program of thruster performance optimization has resulted in significant performance gains for operation about a new set point, defined as a goal for the subject contract effort.

C. PERFORMANCE OPTIMIZATION

As indicated earlier in this report, thruster performance was optimized under the subject contract at a time concurrent with the continuing development (under NASA Contract NAS 3-15385) of the electrostatic vectoring ion extraction system.² Thruster optimization was initiated, therefore, using a first-generation SIT-5 thruster which had been optimized (under NASA Contract NAS 3-14129) for operation with the Model II-1-A electrostatic vectoring system developed earlier.⁸ To optimize steady state thruster operation, the discharge chamber geometry was modified in a systematic manner in order to assess the effect of these modifications on thruster performance. Selective modifications were made in the following thrust-chamber elements:

1. Cathode pole piece geometry
2. Electron baffle size and location
3. Hollow cathode geometry (enclosed and SERT-type configurations)
4. Magnetic field configuration
5. Discharge chamber length
6. Accelerator open area fraction
7. Accelerator open area diameter
8. Neutralizer location.

To permit the magnetic field intensity to be varied as a parameter for optimization, the optimized thruster was equipped initially with a set of 8 rod electro-magnets.

Changes in the cathode cup region, which encloses the main cathode with the cathode pole piece and the electron flow baffle, were critical to changes in discharge-chamber operation. This region is particularly sensitive in the SIT-5 thruster because all of the propellant is introduced through the hollow cathode and passes into the cup region, contrary to the practice of precathode propellant diversion which is common to hollow-cathode thrusters of larger diameter. This technique of propellant introduction can result in performance degradation, unless careful attention is paid to the design of the cathode cup region. There is a tendency for the discharge voltage to decrease as propellant flow through the cathode increases, if the geometrical parameters of the discharge chamber are held constant. Variations of discharge voltage can result in degradation of discharge performance. In the SIT-5 thruster, independent control over discharge voltage has been achieved through the use of postcathode propellant diversion. Ports are located in the walls of the cathode cup pole piece which permit reduction of the neutral particle density below the value which it obtains when these ports are absent. For a given level of beam current, discharge voltage can be regulated by changing the transmission of the propellant diversion ports by the use of wire mesh of varying transparency.

For all optimization testing, mercury flowrate to the main-cathode and neutralizer subassemblies were separately measured with an accuracy of about 1%. Feed tubes from the two vaporizers were connected to separate liquid-mercury reservoirs. For the main cathode, mercury was supplied to the vaporizer from a cylindrical reservoir in which a piston is pressed against the mercury surface to provide the propellant driving force. The piston position is indicated by a dial indicator (calibrated to 0.00025 cm) which contacts the top of the piston shaft and permits accurate determination of the rate of mercury consumption. For the neutralizer cathode, a more sensitive flowmeter was employed which uses a capillary tube (open to atmosphere at the upstream end) to measure mercury consumption. In this system,

mercury is supplied to the vaporizer from a 0.05 mm precision bore capillary burette calibrated in 0.001 cm^3 increments. Displacement of the mercury meniscus as a function of time permits accurate determination of the mercury flowrate. Both feed systems were filled under vacuum in order to eliminate introduction of gas bubbles.

Discharge-chamber optimization of the SIT-5 system was impeded somewhat by the separate development of the beam-extraction system, since discharge-chamber performance is affected strongly by the specific nature of the ion-extraction system with respect to the geometrical open-area ratio, the extraction fields etc.^{9, 10, 11} To minimize this conflict, a beam-extraction system was constructed in a manner which simulated the anticipated geometry of the beam-vectoring system by use of an identical screen electrode in combination with a conventional accel electrode with circular apertures of diameter equal to the separation between vector elements.

In discharge-chamber optimization, the thruster was operated almost exclusively at a discharge voltage close to the maximum acceptable value, and the propellant-utilization efficiency was determined at that operating point alone. These data were sufficient to characterize optimal thruster performance, because both the discharge voltage and propellant utilization efficiency rise steeply together as a function of discharge current.* The value of discharge voltage was restricted to $V_D \lesssim 45$ to limit the rate of discharge-chamber erosion due to ion-bombardment of cathode-potential surfaces.¹³ While preference was given to configurations where high utilization could be achieved with low values of discharge power, only the maximum value of propellant utilization (obtained at maximum discharge power) was considered to be of primary importance, since discharge losses constitute only about 30 to 40% of the total power losses.

* At a given value of ion-beam current, discharge-chamber propellant utilization and discharge voltage are uniquely determined by the discharge current for a particular magnetic and geometric configuration. This is true with all thrusters where total discharge-chamber propellant flow passes through the main cathode.^{5, 10, 12}

On the basis of selective modifications of the discharge-chamber elements available for optimization, a performance peak was identified for operation with the configuration described in Table VI. This configuration was selected initially for operation with the rod electromagnets at a peak axial magnetic-field strength of 53 gauss, one-half the intensity recorded for operation with the 8 permanent magnets which were chosen on the basis of scaling from the SERT-II geometry.

TABLE VI
Key Parameters for Optimized Thruster Operation with
Simulated TV Optics

Main Keeper Aperture	
Diameter	0.475 cm
Thickness	0.051 cm
Neutralizer Keeper Aperture	
Diameter	0.081 cm
Thickness	0.025 cm
Neutralizer Position	
Neutralizer pointing angle with respect to the thruster axis	0°
Distance from the keeper aperture from the outermost beam aperture	
Downstream	3.55 cm
Radially outward	2.36 cm
Baffle	
Diameter	0.952 cm
Radial Gap	0.159 cm
Axial Gap	0.159 cm
Transmission of Mesh Covering Propellant Diversion Ports	91%
Magnetic Field Generation	4 magnets (0.450 cm diameter) equally spaced
Length of Collar Pole Piece	0.952 cm

T928

For subsequent thruster tests, a magnetic-field pattern similar to the one generated with the electromagnets was provided by substitution of four permanent magnets (0.450 cm in diameter) equally spaced at every second position identified in the design for the eight-magnet configuration. * In the final SIT-5 design, the four sets of unused magnet-retainer clamps were left in place and stainless steel rods were placed at the unused magnet locations to preserve azimuthal structural symmetry. In this configuration, the thruster was operated for over 46 hours at the performance level indicated in Table II with a beam current $I_B = 25.6$ mA, a discharge-chamber propellant-utilization efficiency $\eta'_m = 82.5\%$ and an electrical efficiency $\eta_E = 56\%$ at a discharge voltage $V_D = 45$ V. Similar electrical performance was demonstrated at a discharge voltage $V_D = 42$ V with $\eta'_m = 79.9\%$.

1. Neutralizer Orientation

At the request of the NASA Project Manager, the neutralizer cathode was reoriented from its earlier location, so that the aperture of the neutralizer-keeper electrode was placed at a position 2.71 cm downstream and 2.71 cm radially outward from the outermost beam aperture of the ion-extraction system with the axis of the neutralizer cathode directed straight downstream parallel to the thruster axis. At the conclusion of the thruster optimization program, the SIT-5 thruster was operated with its neutralizer in the straight configuration to insure that adequate coupling characteristics were obtained with the beam plasma.

Coupling characteristics with the straight neutralizer configuration generally similar to earlier operations (reported for thrust-vector operation under NAS 3-14129) when the neutralizer axis rotated by 60° toward the beam axis and with the aperture on a line extending at 17° with the thruster axis from the outermost beam

* This arrangement does not place the four magnets in position of azimuthal symmetry with respect to the thrust-vectorable ion-extraction system.

aperture.¹ The only significant difference in the current performance is the somewhat higher value of neutralizer propellant flowrate $I_{N, Hg} = 2.6$ mA required to hold the neutralizer keeper voltage within the limit $V_{N, K} < 20$ V recommended by the NASA Project Manager. This variation is attributed to the enlarged keeper aperture and is not thought to be related to neutralizer orientation. The new neutralizer configuration was adopted, therefore, for incorporation into the optimized SIT-5 thruster configuration.

2. Structural Optimization

In the analysis and design which preceded construction of the SIT-5 system (under NASA Contract NAS 3-14129 and NAS 3-14058), the unambiguous goal was that of avoiding catastrophic failure during the structural integrity test. No opportunity had been provided under the above mentioned programs to optimize the structural design. This effort has now been undertaken as part of the subject contract.

a. Dynamic Modeling

To initiate the structural optimization process, accelerometer response data generated during the earlier vibration tests (under NASA Contract NAS 3-14129) were reduced and analyzed. By comparing observed responses at a given location with the responses predicted by dynamic analysis, the analytical mathematical model generated under the earlier program was improved and corrected as required, to match prediction with observation. The revised mathematical model was used as a precision instrument to predict dynamic loads with a high degree of confidence. New design concepts were factored into the existing mathematical model, because the accuracy of the dynamic description of each of the structural elements depends not only on the matrix describing that particular element, but also on the dynamic environment represented by all other elements with which it is coupled. Proceeding from an accurate model of an

existing system, the effects of modifications in particular structural elements could be evaluated.

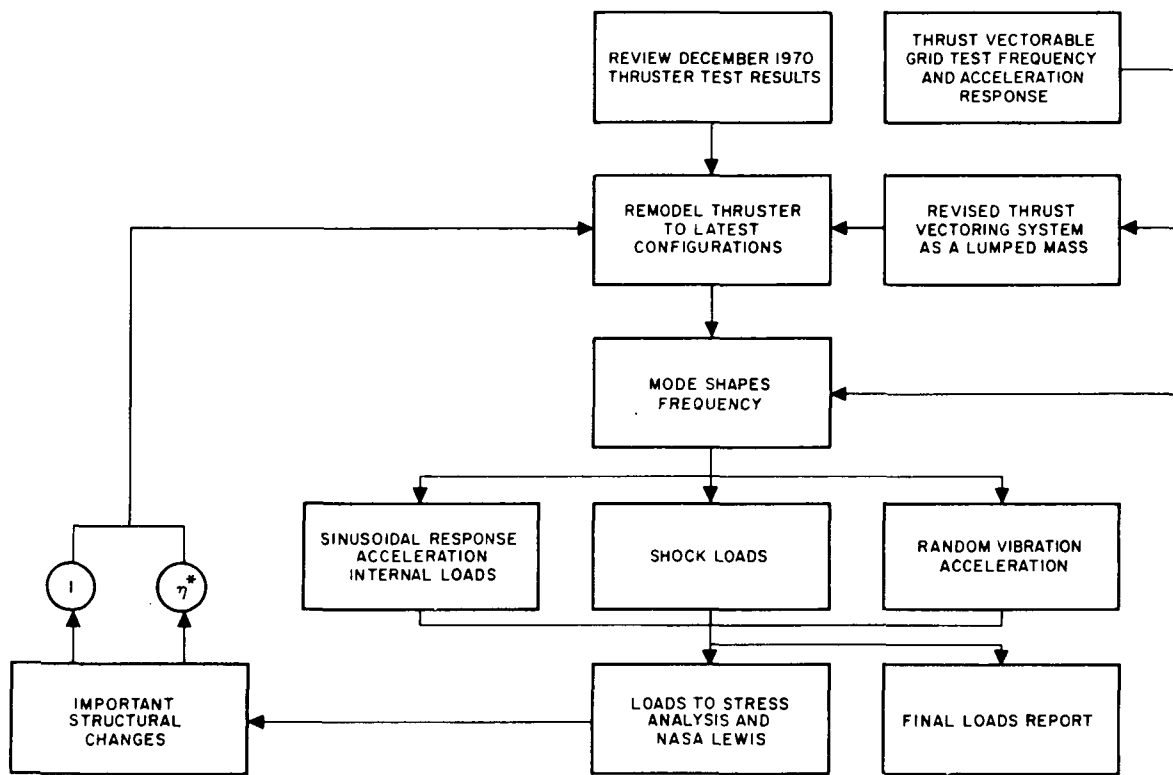
Details of the analytical procedure are outlined in the flow chart shown in Fig. 8. This procedure permits continuous updating of previously generated, lumped-mass dynamic mathematical models. Application of the information derived from the vibration tests through this procedure provides a basis for recommending new thicknesses for use with major structural components. New thicknesses, together with geometry, material, and mass changes are incorporated as further revisions of the mathematical model.

As in the previous analyses, frequencies and mode shapes for the new thruster design were generated. These mode shapes and frequencies were examined to determine if any changes to the structure could be initiated before proceeding with the response loads portion of the analysis. Areas which exhibited low frequency (indicating lack of structural rigidity for critical components) were changed at this point, and the mode shapes and frequencies were calculated before the dynamic response was analyzed.

A dynamic response analysis was then carried out using the calculated mode shapes and frequencies and the forcing functions of the contract specification. Sinusoidal and random vibration, as well as the shock spectrum environment, provided the forcing functions. Response accelerations and displacements for all unrestrained degrees of freedom were calculated for each mass station and used for stress analysis. In addition, internal loads on the flexible structural elements connecting the mass stations were calculated for the sinusoidal as well as the random environments. A formal load document was published¹⁴ and forwarded to the NASA Project Manager for his approval.

b. Stress Analysis

From the accelerations and displacements predicted by the loads document, dynamic and static stresses were calculated for the SIT-5 structure. Stress profiles were analyzed to identify



*7 = 0-2

Fig. 8. Analysis flow chart for SIT-5 redesign.

areas in the mechanical design where modifications were appropriate to further the goal of system optimization with respect to strength, rigidity, and minimum mass. As shown in Fig. 8, changes implemented as a result of this analysis were introduced as modifications in the mathematical model to determine new modes and frequencies appropriate to the changed configuration. By this procedure, the dynamic loads predicted by mathematical analysis were made consistent with the current configuration. The results of this analysis were summarized in a special report¹⁵ and submitted to the NASA Project Manager for his approval. Significant results of that analysis are described below.

Several alternate design concepts were evaluated for mounting the ion engine to a space vehicle. Two candidate types of flanges which were investigated were the axially-oriented ring flange with bolts in shear, and the radially-oriented ring flange with bolts in tension and bending. The axially oriented ring flange was selected as superior to the radial flange because of the following reasons:

- The attachment bolts are stressed in shear which minimize problems associated with torque and locking.
- Moments are transmitted as shear couples on a plane. This offers a stiffer path than that provided by tension and bearing couples.
- Local stress levels transmitted to the spherical shell members (reservoir structure), are minimized due to shorter moment arms.

For fastening to the axial flange, three types of attachments were considered; namely, the Keensert,^{*} floating nut plate, and threaded hole. The Keensert type of attachment was selected because it is simpler to install, and because the floating nut requires additional clearances for its larger dimensions. The threaded hole was rejected because it would be subjected to potential galling and thread stripping with repeated installations.

* Keensert is a trade name for a threaded insert manufactured by the Newton Insert Co., Los Angeles, California.

Three types of designs were evaluated for the structure which supports the thruster from the region of the mounting flange:

1. A conical monocoque shell attached to the engine mounting flange by shear bolts
2. A stiffened monocoque shell mounted to the mounting flange by shear bolts
3. A stiffened conical shell with cutouts.

The conical monocoque shell design was selected for the thruster support structure primarily because of its simplicity. Its weight is comparable to the other two designs because of the reduced dimensions. A minimum thickness gauge of 0.020 inches was selected, based on handling loads and local bearing stress considerations. The thruster support structure is basically cantilevered from the engine mounting flange. It is designed to carry and transmit loads from the thruster components (neutralizer, vaporizer, screen, etc.) to the ring mounting flange. Stress analysis also considered column stability and secondary stresses caused by local cutouts from the pressure transducer and fill valve.

The stress analysis of the thruster support structure was implemented by the HAC shell computer program. This program is based on the finite element method for the determination of stresses, strains, and displacements. The local stress concentrations on the main thruster shell resulting from the applied loads of the pressure transducer and fill valve inertia loads were determined using the Bijlaard method of analysis.¹⁶ A combination of 150 G axial and 150 G lateral acceleration load factors for the pressure transducer loads were used as a conservative estimate of the combined inertial forces acting on the structure.

3. Design Modifications

The major goals of the redesign effort were to reduce assembly difficulties encountered with the earlier effort; minimize system mass,

reduce fabrication problems, and to integrate the new thruster with the electrostatic thrust vectoring extraction system. These goals were satisfied in the second-generation system by the following modifications:

a. Main Connecting Structure — The main connecting structure was redesigned to an azimuthally-symmetric configuration which minimizes over-all mass while permitting removal of the structure without disconnecting the mercury feed lines. As part of the mass reduction, electrical terminal blocks were replaced with individually insulated terminals located along the circumference of the main connecting structure.

b. Propellant Reservoir Subsystem — An all-welded construction is adopted in the redesigned propellant reservoir subsystem. In the new design, the bladder "O" ring is held in compression by structures which are stressed mainly in shear with minimum moment for bending or tearing strains. Redundant protection is provided against leakage of propellant and/or gas pressurant, because the bladder is totally enclosed within a constant-pressure metal envelope.

c. Thrust-Vector Grids — From the inception, this system has been designed for integration with the thrust-vectorable extraction grids. Modifications were made in the shape and position of the ground-screen mask, and increased standoff capability is provided by the high-voltage isolator.

d. Neutralizer — The aperture of the neutralizer keeper electrode is located 2.71 cm downstream and 2.71 cm radially outward from the outermost beam-forming aperture of the ion-extraction system. The neutralizer subassembly points directly downstream in a direction parallel to the thruster axis. The neutralizer-vaporizer subassembly is shown in Fig. 9, attached to its integral enclosed keeper electrode. The unit is fastened redundantly at the cathode and vaporizer location with metal brackets. Because of its low over-all mass, the entire assembly is supported directly by the cylindrical structure of the ground-screen shroud.

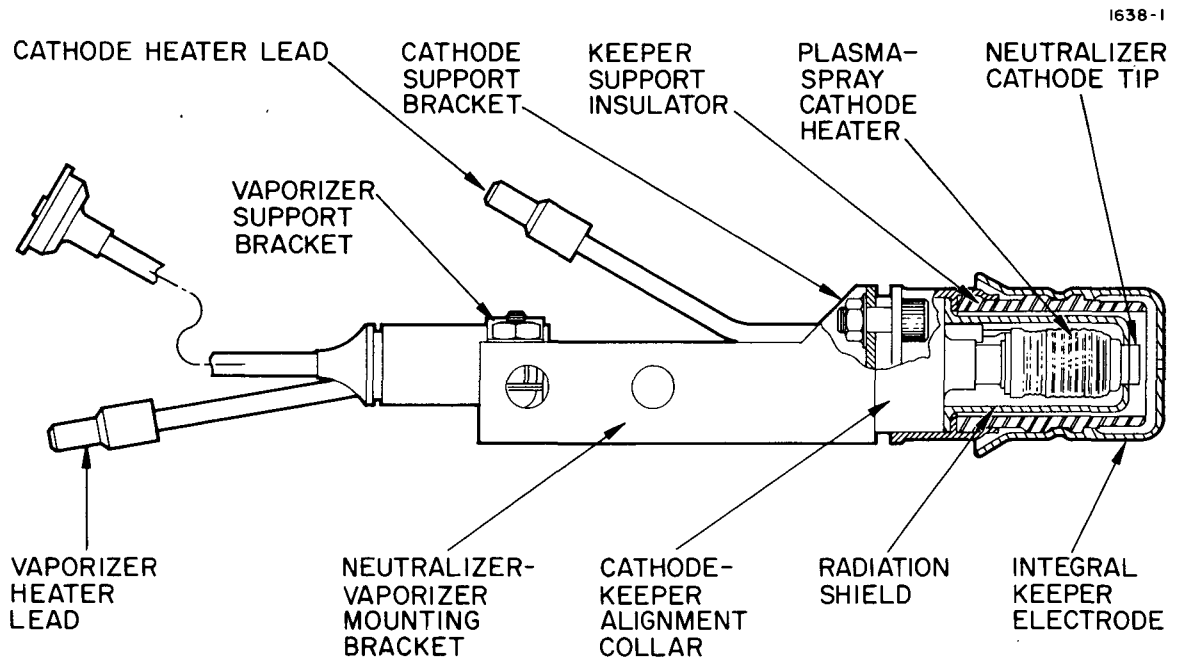


Fig. 9. Neutralizer-vaporizer (NV) subassembly with integral enclosed keeper electrode.

e. Main Keeper Assembly — For ease of fabrication, the main keeper (shown in Fig. 10) employs a swaged metal-to-ceramic joint instead of the metal to ceramic braze used earlier. Accurate registration of critical dimensions is assured by stepped ridges provided on the metal elements.

f. Cathode Heater Design — A fabrication technique was adapted for use at HRL in which a tungsten-rhenium heater element is attached directly to the cathode tube by plasma-spray encapsulation with alumina. This fabrication was adapted from the considerably larger heater design that was developed at the Lewis Research Center for use with the SERT II thruster system.³ This technique of fabrication is thought to utilize the best available combination of materials from the standpoint of chemical compatibility during high temperature operation. To minimize the possibility of chemical attack during high temperature operation, a protective coating of tungsten separates the tantalum cathode tube from the base coating of plasma sprayed alumina. As shown in Fig. 11, tantalum is permitted to contact the alumina only at the somewhat cooler location of the tantalum attachment band, which provides a stable surface for joining the 0.010 in. diameter tungsten 25% rhenium heater wire with the tantalum center conductor of the heater lead. The tantalum termination strap at the other end of the restrictive element is attached directly to the cathode tube beyond the region of alumina coating.

g. CIV Subassembly — An area of experimental difficulty encountered during optimization testing bears special mention, because of its general application to existing hardware. Although the seals and welds of all CIV subassemblies are checked for vacuum integrity (with a helium leak detector) prior to thruster operation, hairline cracks were found to develop in sensitive regions after service at operating temperature. This problem was first indicated by otherwise inexplicable variations in propellant utilization efficiency when different CIV's were used with the same discharge chamber and also by occasional decreases in utilization with the same experimental apparatus

M8517

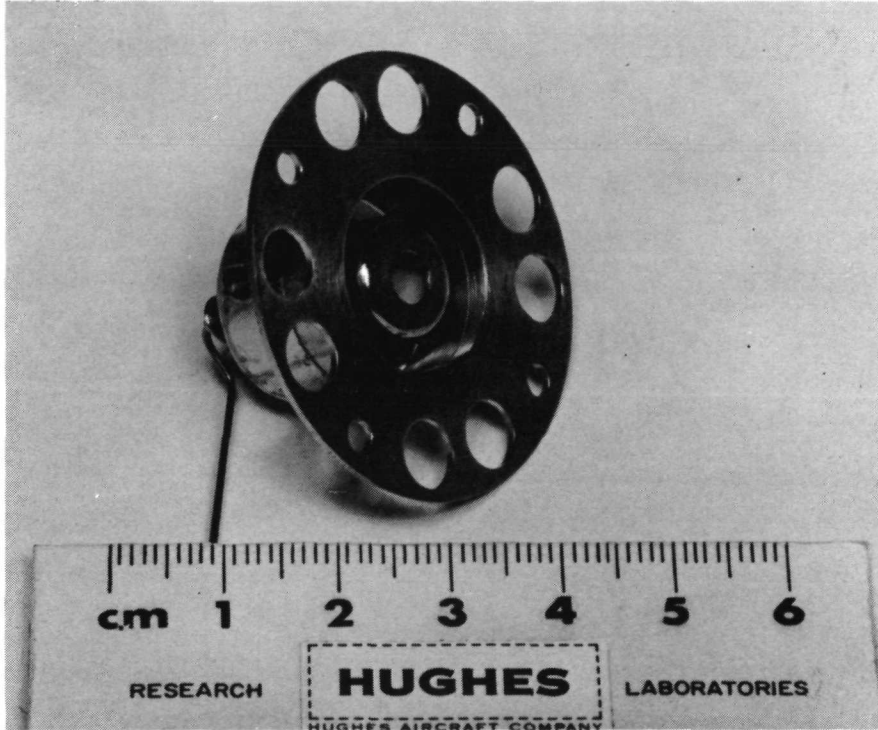


Fig. 10. SIT-5 CIV subassembly with swaged metal to insulator connection.

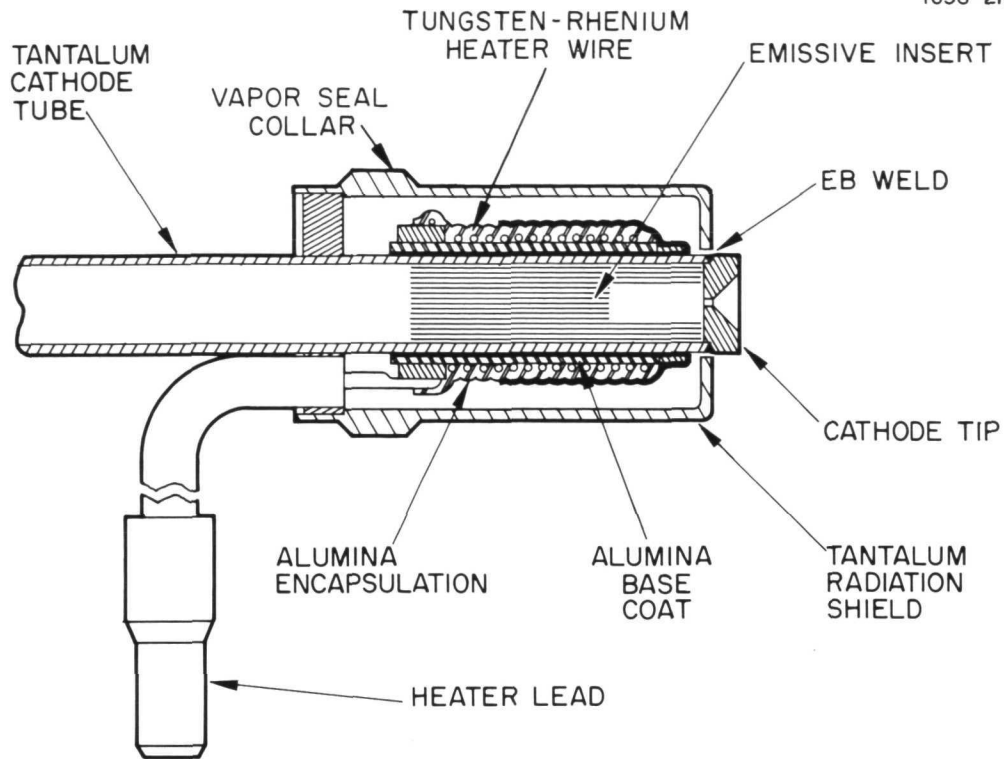


Fig. 11(a). Hughes hollow cathode subassembly.

M8518

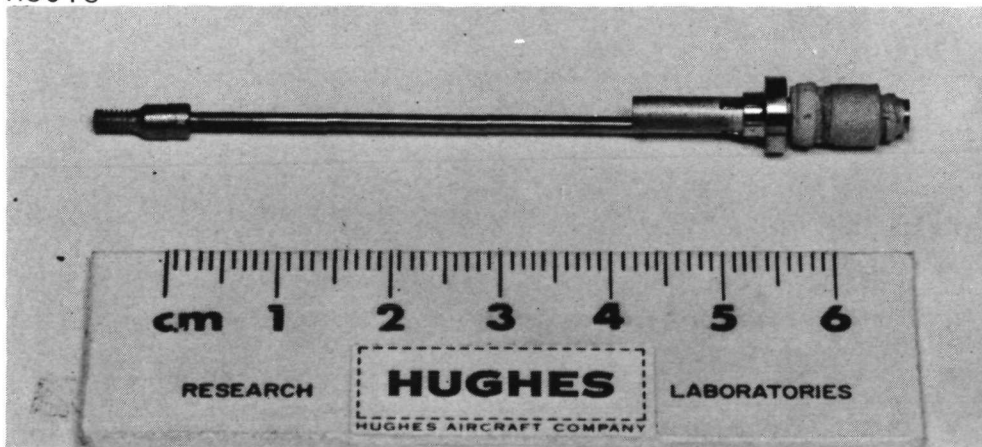


Fig. 11(b). SIT-5 cathode with plasma spray alumina encapsulated heater element.

from one test day to the next. The cause of this problem has now been identified as arising from an incompatibility in the welding characteristics of tantalum with stainless steel and has been avoided in future fabrication by design modifications.

The major area of concern with respect to propellant leakage occurs in the main vaporizer liquid housing shown schematically in Fig. 12. In the original design, the liquid housing and propellant feed tube were fabricated of stainless steel, while the vaporizer-plug housing was made of tantalum to match its welding characteristics with those of the porous-tungsten vaporizer plug. Because of the vast difference in material properties of the two substances, the weld of the stainless steel liquid housing with the tantalum plug housing had at first been viewed with considerable apprehension. By using a lapped configuration in the weld region, however, consistent attachments were achieved with no leaks being detected. After successful completion of the Structural Integrity Tests with a CIV subassembly of this design, (under Contract NAS 3-14129), the integrity of the weld seemed to be confirmed.

The presence of hairline cracks in the stainless steel-to-tantalum weld was postulated initially as the only plausible explanation for observed variations in thruster propellant utilization efficiency η_m when different CIV's were used. It was argued that very small openings in the liquid side of the vaporizer housing could result in significant losses of mercury vapor when the vaporizer is at its operating temperature even though no liquid leakage is observed. Liquid mercury is not transmitted through small capillary passages because of surface-tension forces, however, vapor flux is readily transmitted through the passage at a rate proportional to the area of the opening. While this area may be quite small, it enjoys a ten thousand to-one competitive advantage over vapor passage to the discharge chamber through the much larger vaporizer area, because of the low transmission coefficient of the vaporizer plug. The presence of these capillary cracks was later confirmed by rechecking the CIV subassemblies with the helium leak detector after many hours of use at normal operating temperature.

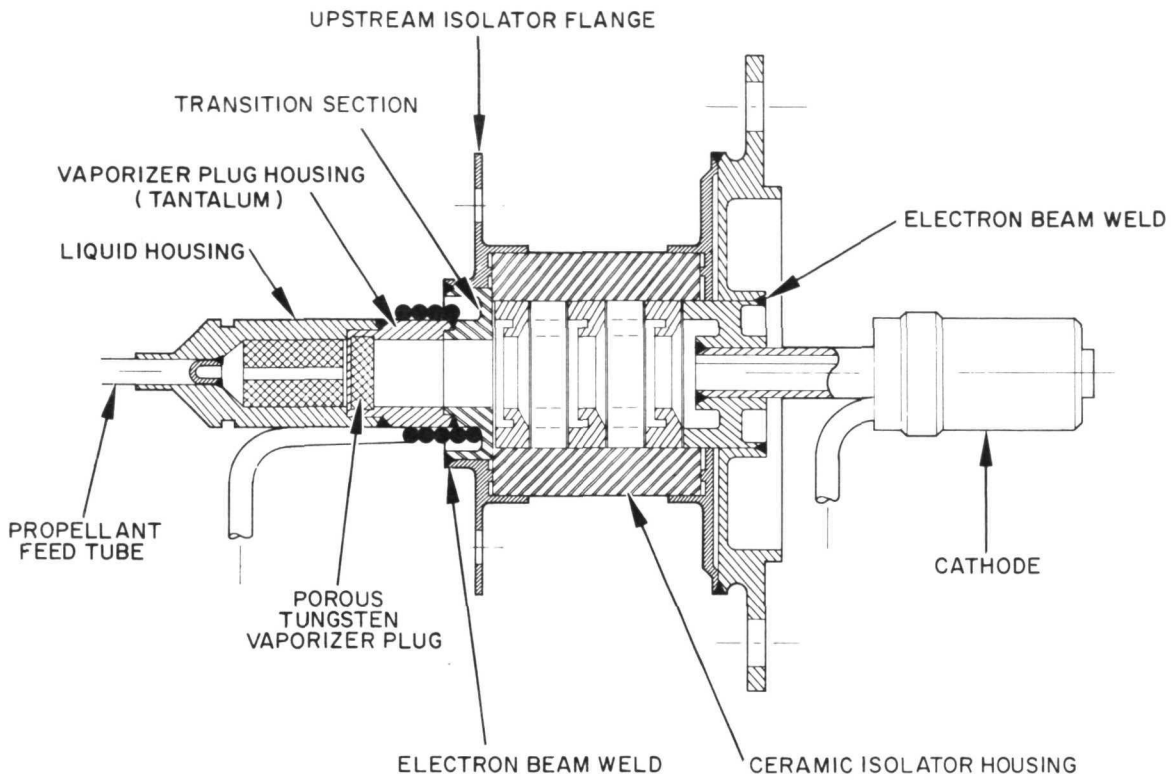


Fig. 12. Engineering drawing of SIT-5 CIV.

Subsequent fabrication of CIV subassemblies have avoided this weakness by a change redesign which calls for the use of tantalum throughout the liquid side of the vaporizer subassembly from its attachment to the propellant reservoir to the location of the vaporizer plug. The use of tantalum is extended throughout the region upstream of ceramic isolator housing. This has been shown to be feasible by the successful completion of leak tight copper brazes between the ceramic isolator housing and an upstream isolator flange fabricated of tantalum. In this configuration, the vaporizer plug housing and the transition section are fabricated from a single piece of tantalum.

D. TEST QUALIFICATION

An extensive program of system testing has confirmed design expectations with regard to structural integrity and steady-state and cyclic performance capabilities. In its optimized discharge-chamber configuration (including electrostatic thrust vectoring optics), two thrusters were constructed and submitted to a Launch Environment test after which one of them was operated under steady-state conditions to establish system performance after launch simulation. An identical thruster was operated under cyclic conditions to qualify the system for its intended application for attitude control and station-keeping of synchronous satellites.

1. Launch Environment Test

Both the S/N 201 and S/N 202 modules of the SIT-5 thruster system were tested for structural integrity by subjecting the units to a simulated launch environment of $\pm 30G$ shock, 9 G sinusoidal, and 19.9 G rms random vibration. No major structural failures were encountered during the tests; however, several lesser failures and deficiencies were uncovered which have now been corrected by straightforward design changes. The structural soundness of some of these

changes has already been indicated by their successful implementation into the S/N 202 thruster module prior to the end of the Launch Environment Tests. In the discussion which follows, test observations are described which have helped to identify mechanical deficiencies in the design and/or workmanship of the tested SIT-5 units. In each case, corrective actions are described which have been implemented to rectify these deficiencies.

a. Thruster Support Insulators

● Test Observations

Upon post-test disassembly of the S/N 202 unit, a partial failure was uncovered that has resulted in a significant design improvement that has already been incorporated into both thruster units. When the locknuts were released which fasten the thruster flange and endplate to the four support insulators, in both thruster modules two of the insulators were found to be fractured at the point where they are brazed to Kovar sleeves as shown in Fig. 13. From the amount of abraded metal which blackened the contacting fracture surfaces, it was apparent that vibration testing had continued for a significant time after these fractures had occurred without consequent failure of the support structure. This resistance to further damage points out the more than adequate strength of this structure. The fact that fracture did occur, however, has indicated an area where design improvements should be made.

● Corrective Action

A redesigned configuration has now been implemented which increases the strength of the support structure by an order of magnitude, because it permits all thruster mounting ceramics to be held in compression both during assembly and under peak-load conditions. As shown in Fig. 14, the design concept is sufficiently straightforward that it has even been possible to incorporate it into both the S/N 201 and S/N 202 units while using the same set of support insulators. The four thruster support insulators are held in compression by pressing them (by means of central stainless-steel lugs) against

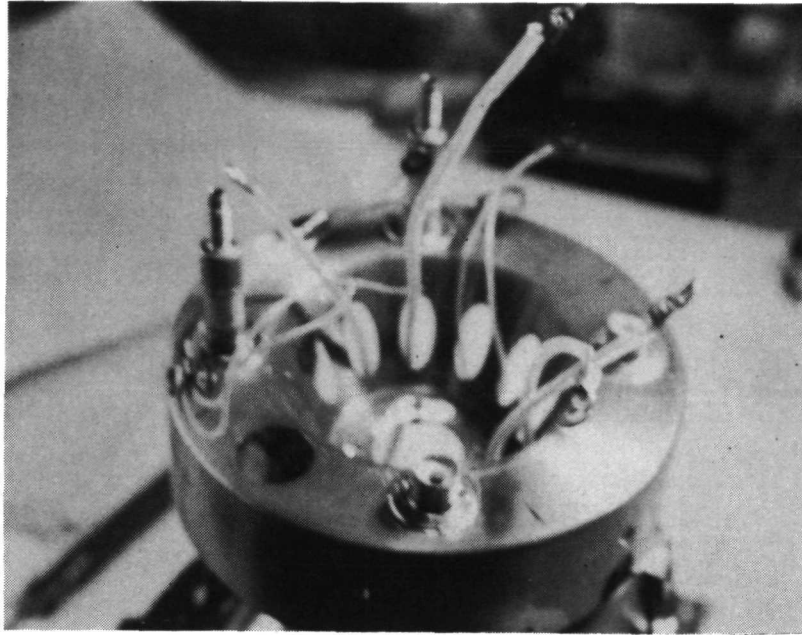


Fig. 13. S/N thruster showing fracture of two ceramic support insulators.

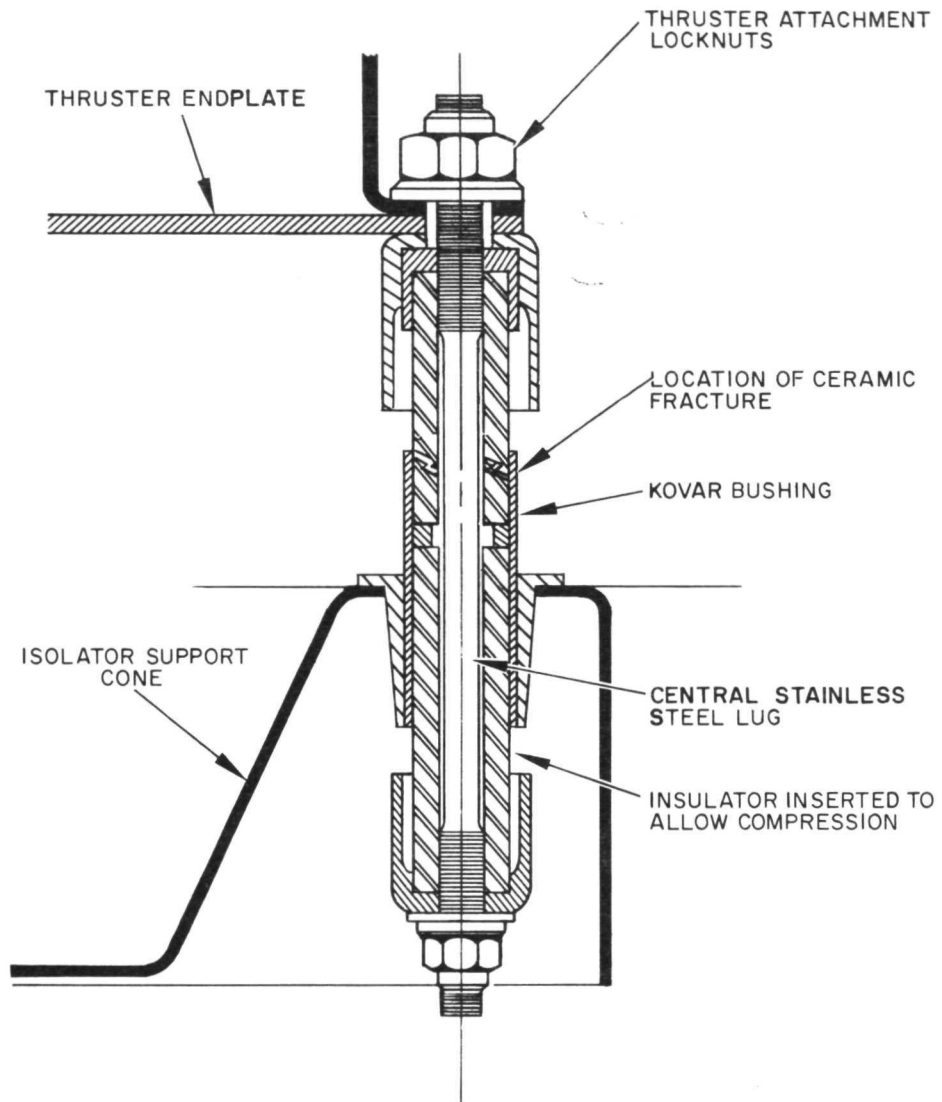


Fig. 14. Redesigned thruster support insulators.

a second set of four insulators which are inserted from the opposite side of the Kovar bushings. Since the two ceramic fractures occurred slightly inside of the bushings, all eight ceramic tubes are restrained from transverse motion. With all four thruster support insulators placed in compression by this expedient, it is possible (in the final assembly) to insure that the isolator ceramic is also placed in compression without placing the support insulators in tension.

b. Neutralizer-Vaporizer Feed Tube

- Test Observation

Testing of the S/N 202 system was terminated prematurely by separation of the neutralizer-vaporizer feed line due to the stress embrittlement at its reservoir adaptor flange. The possibility of this mode of failure in both units had already been communicated to the NASA Project Manager before beginning either launch environment test when it was discovered that insufficient length had been allotted at the time of fabrication of the neutralizer feed tube so that it was extended in a straight line from the reservoir manifold to the neutralizer vaporizer without the benefit of stress-relief loops as provided with the CIV feed line and mercury fill line. While it was realized that testing under these conditions would encounter a calculated risk, a mutual decision was made at that time to proceed with testing rather than accept the one-month delay anticipated for the fabrication of additional hardware.

- Corrective Action

Design corrections have been made to prevent future failure of the neutralizer-vaporizer feed line. Two stress-relief loops have been provided (one at each end of the feed line) to decouple vibrations in the unsupported length of the feed line from the region of the end connections. These loops are oriented in separate planes to decrease the sensitivity for planer vibration.

c. Thrust – Vector-Optics' Sputter Shields and Electrical Leads

- Test Observations

Dynamic testing of the S/N 201 thruster was relatively uneventful except for the stress-embrittlement failure of two solid-nickel lead wires and of all four of the stainless-steel sputter shields which surround the ceramic insulators of the thrust-vector optics. The S/N 201 thruster is shown in Fig. 15 after completion of all dynamic testing.

- Corrective Action

The structural integrity of corrective design changes has already been indicated by testing with the S/N 202 unit. No stress embrittlement was detected when the solid wires were replaced in the second unit by braided stranded wire, and the 0.005-inch thick sputter shields were reinforced at their attachment points by 0.016 inch thick stainless steel stiffeners.

d. Loose Parts

- Test Observation

Near the conclusion of the final sinusoidal vibration test of the S/N 202 module, a loose nut was noted inside of the ground screen enclosure. The ground screen was removed, and a 2-56 locknut was taken out. This nut was assumed to have dropped in during thruster assembly, since no nuts were missing from any of the thruster subassemblies. During this inspection, a crescent shaped metal sliver was also discovered. The metal piece which is shown in Fig. 16 had apparently broken loose from the foot of one of the magnet retainer clamps at the location where it joins with its collar which is swagged to the magnet. This sliver was still held to the thruster end flange by magnetic attraction, but had migrated to the periphery of the end flange where it bridged the gap which separated the thruster from a nickel wire leading to the ion-extraction system.

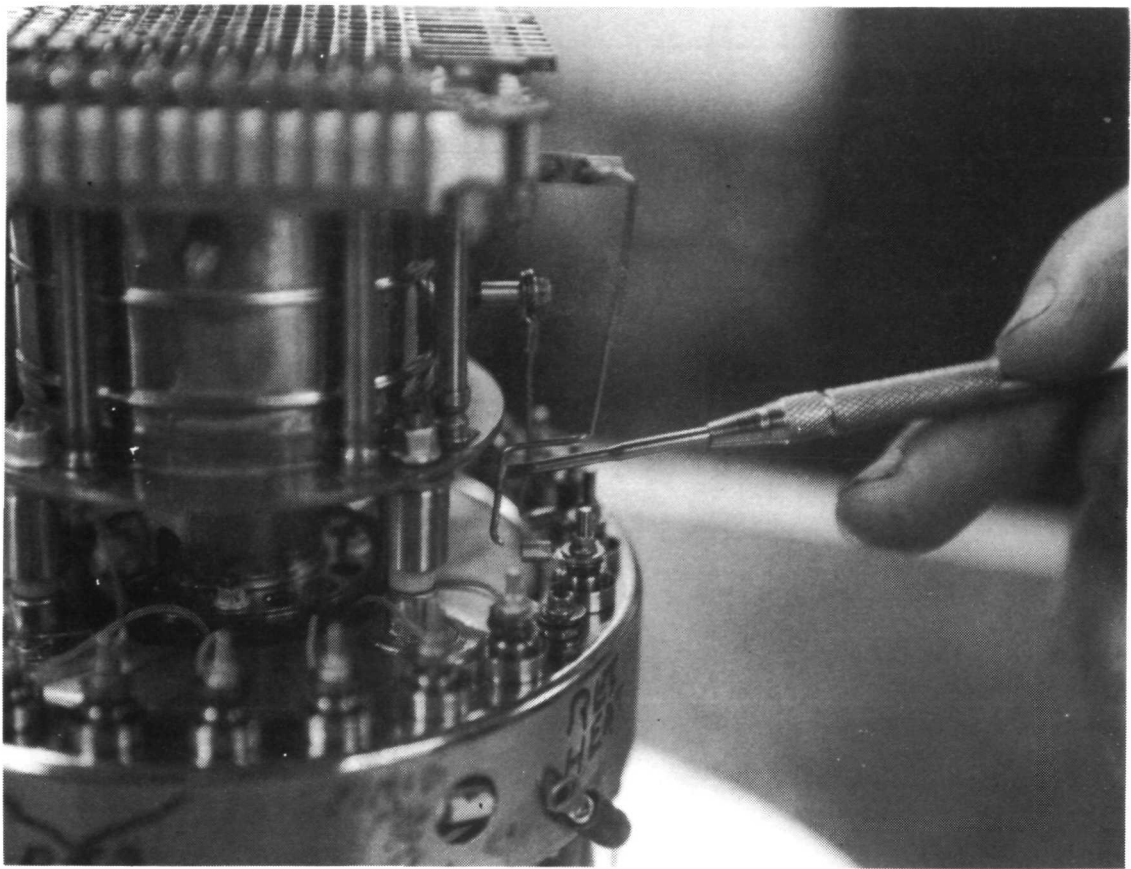


Fig. 15. S/N 201 thruster showing loss of optics sputter shields and fracture of solid-nickel lead wire due to stress embrittlement.

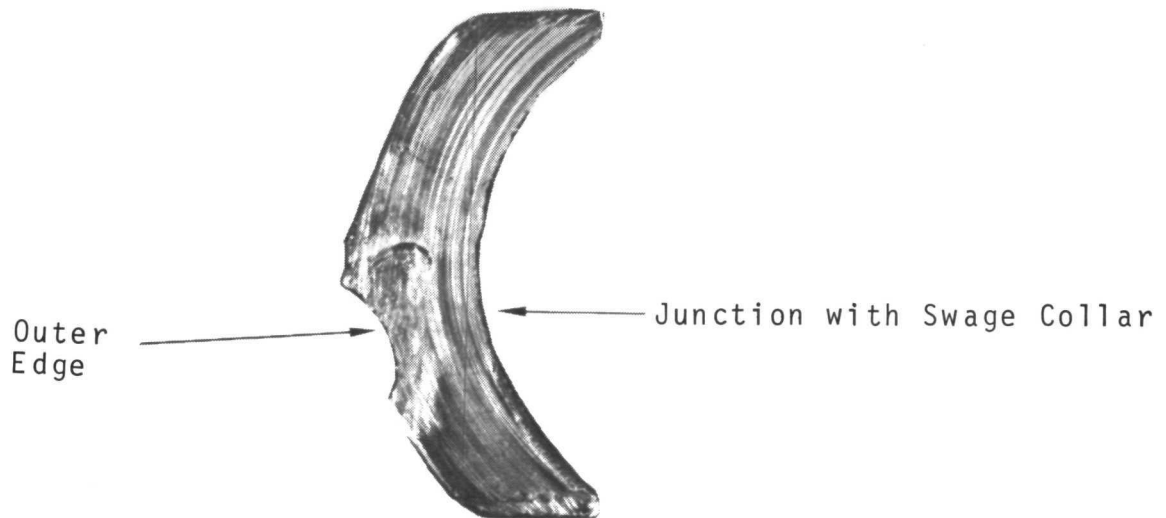


Fig. 16. Metal crescent which broke loose from the foot of a magnetic retainer clamp.

- Corrective Action

The attraction of the metal crescent to the nickel wire pointed out dramatically that magnetic materials must not be used for electrical leads in applications of this type. As an alternative, braided tantalum wire has been chosen for use in future applications.

Future fractures of the magnet-retainer clamps are avoided by providing a sufficient radius of curvature at the junction between the base region and the circular swage collar to reduce the stress concentration which occurs at that point. Also, the base thickness has been increased from 0.015 inches to 0.025 inches.

e. Ground Screen

- Test Observation

Early in vibration testing of the S/N 202 module, the test was temporarily terminated by the progressive failure of the perforated ground-screen enclosure by shredding along the lines of perforation. This damage was first detected by the unusually metallic sound of the thruster system during random vibration, but the cause was not identified until after about two minutes of full-level vibration at which time the test was stopped. Visual inspection at that time showed that a small piece of material had already torn away from the ground screen in the vicinity of the neutralizer support bracket as shown in Fig. 17. Manual testing of the ground screen enclosure indicated that this violation of its cylindrical integrity had severely weakened the structure to the point that the ground screen mask and neutralizer subassembly were inadequately supported and may have undergone excessive displacements.

- Corrective Action

The cause of the ground-screen failure was at first thought to reflect a design deficiency, but has since been identified as an error of quality control. Post-test measurements have shown that the nominal 0.008-inch thick perforated ground-screen material

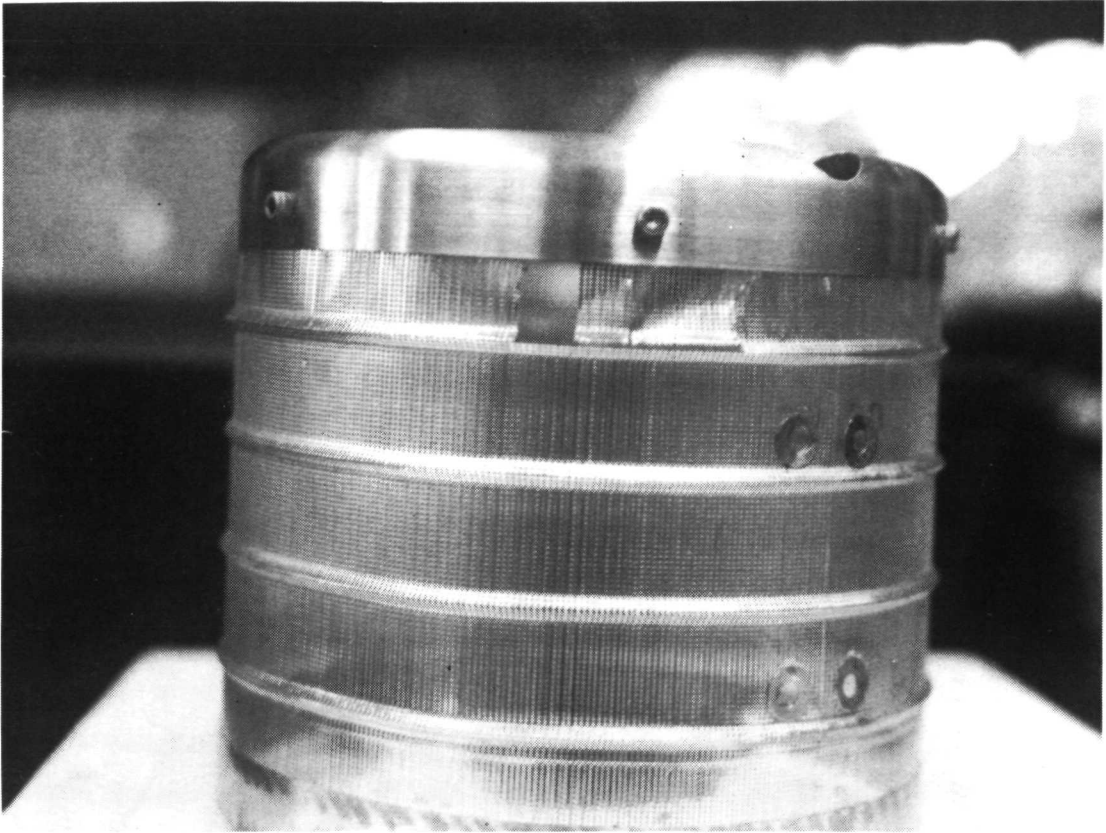


Fig. 17. Ground screen of S/N 202 thruster showing material shredding and the loss of a small piece of screen.

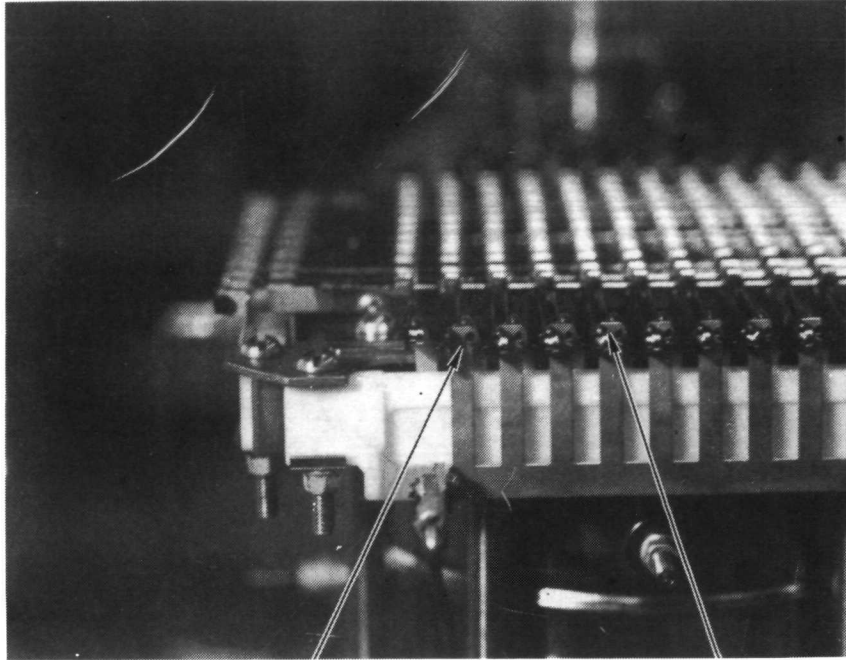
was, in fact, less than 0.006 inches in thickness. It is believed that this variance has resulted from excessive chemical erosion during electropolishing of the material. Even at this thickness, however, the problem appears to be obviated by a design innovation incorporated into a spare ground screen. Subsequent testing with the S/N 202 system using the modified ground screen showed no sign of material tearing or shreading when the perforated material was reinforced by 1/2 inch bands of 0.010 inch thick stainless steel stock, which were spot-welded at each end of the perforated cylinder. By terminating the rows of perforation in this manner, tearing action is avoided and the integrity of the cylindrical surface is maintained.

For future fabrication, a new procedure for manufacture of the ground screen has been adapted. In the new design, perforations in the ground screen are provided (as required for vacuum venting) by photoetching a solid 0.008 inch stainless steel sheet. Solid regions are retained as required for structural strength. Finally, the sheet is rolled into a cylindrical shape and completed as before by beam welding the seam and forming stiffening ribs at selected locations.

f. Accel Grid Element

● Test Observation

After completion of dynamic testing of the S/N 201 unit, one of the 44 accel grid elements was found to be loose at one end. As shown in Fig. 18, this was due to loss of the pin that attaches it to its spring-tension support finger. Visual inspection confirmed that this pin had not properly been brazed to the element. This problem was created by a deficiency in quality control over the brazing process which had already been corrected in manufacture of subsequent units of the thrust-vector optics.



Missing Pin Location

Other Pins Still in
Place

Fig. 18. Thrust vector optics S/N 601 after vibration test on SIT-5 thruster S/N 201.

• Corrective Action

An examination of the time history of this particular optics assembly shows the following main events.

- a) Initial assembly of the optics on thruster.
- b) Thruster operated for approximately 100 hours under NASA Contract NAS 3-15385.
- c) Optics disassembled and cleaned after performance test by:
 - 1) Light sandblast to remove any sputtered material.
 - 2) Electropolished to further clean surface of accel strips.
 - 3) Ultrasonically cleaned in alcohol and dried in gaseous nitrogen.
- d) Optics reassembled on thruster S/N 201.
- e) Vibration test.

The cause of failure was considered to be two-fold. During the initial assembly of this optics, it was observed that the chromium oxide formed on the 304 stainless steel pins was sufficient to prevent proper wetting of the Silcoro brazing material at 875°C. In subsequent assemblies, this problem has been solved by nickel plating (0.0002 inch) the stainless steel pins prior to the brazing operation. This procedure was initiated with the S/N 602-S/N 606 optics assemblies prior to the time of vibration-test of the optics themselves under NASA Contract NAS 3-15385 and was then recognized as a potential weakness in the earlier assembly process. Secondly, during the electropolishing procedure, it is probable that the boundary of the brazing material is preferentially etched and more material is removed from this area. This is an unusual procedure and was unique only to the optics assembly S/N 601 and should not be cause for concern on other assemblies.

g. Neutralizer-Keeper Attachment Flange

● Test Observation

In both the S/N 201 and S/N 202 modules, some loosening was detected in the swagged stainless steel-to-ceramic attachment which joins the neutralizer-keeper insulator with its stainless-steel attachment flange. This effect is felt to be of little importance, and no repair was necessary in preparation for thruster performance testing.

● Corrective Action

To increase the strength of the swagged metal attachment for future fabrications, the length of the cylindrical flange collar has been increased.

2. Steady State Performance Test

After completion of the Launch Environment test, a Durability and Performance Mapping Test was carried out in an oil-diffusion-pumped vacuum system approximately 5 feet in diameter x 15 feet long. This chamber has a cylindrical liquid-nitrogen cooled liner. The SIT-5 module was located on the axis of the chamber and mounted directly to a chamber end plate. A stainless-steel water-cooled beam collector is located at the opposite end of the chamber. The chamber also contains a movable ion-beam scanner that was used to measure beam deflections by the electrostatic deflection system of the thruster. The pressure in the chamber did not exceed 5×10^{-7} Torr during the tests.

a. Durability Test

Initial startup of the SIT-5 module after the Launch Environment test presented no major problems. Startup of the main keeper discharge occurred with a keeper voltage of 500 volts while the neutralizer keeper discharge required a somewhat higher starting

voltage (4 kV) for its primary ignition (both with 20 W applied to the cathode-tip heater). After the durability test was under way, subsequent neutralizer restarts were accomplished with 500 volts with 20 W of heating. The duration of the durability test was taken to be only the beam-on time; this was a total time of 165 hours. Only two interruptions occurred after the start of the durability test. The first was intentional and occurred early in the test for about 1 hour to install a main vaporizer controller. The second interruption occurred midway through the test for about 6 hours, because of a high-voltage arc which actuated a protective circuit that is used to shut off all power (except to the vaporizer) should 10 mA of current be drawn by the accel supply. Restart of the system presented no problems. The unreduced data sheets were transmitted to the NASA Project manager as part of a special report.

Performance parameters were recorded throughout the test. Three sets of values are shown in Table VII that were taken at the end of 70 hours, 114 hours and 157 hours of operations. These values were taken just prior to obtaining measurements of beam deflection data. Table VII shows that the system provided a thrust $T = 0.46$ mlb at a net accelerating voltage $V_B = 1600$ V with a propellant utilization of 73% (including neutralizer and startup losses) and a system electrical efficiency $\eta_E = 51\%$. It can be seen that all three sets are nearly identical.

The main vaporizer and neutralizer vaporizer have a common feed system; therefore, only the total amount of mercury consumed during the test is known. The average total mercury equivalent flowrate is obtained from the mass consumed and duration of the test. Since this value was calculated by averaging over the time the beam was actually on, it is thought to represent a conservative value. No corrections were made for startups or for a one-half hour operation with beam-off and main discharge on.

TABLE VII

SIT-5 (S/N 201) System Performance Profile

Nominal Operating Parameters	After 70 Hr	After 114 Hr	After 157 Hr
Beam Voltage, V	1600	1600	1600
Beam Current, mA	25	25	25.1
Accel Voltage, V	-800	800	-800
Accel Drain Current, mA (at 0° deflection)	0.080	0.075	0.080
Discharge Voltage, V	45	44.6	45
Discharge Current, mA	367	365	363
Discharge Power, W	16.5	16.3	16.3
Cathode			
Keeper Voltage, V	14.8	15	15
Keeper Current, mA	370	370	370
Keeper Power, W	5.5	5.6	5.6
Heater Power, W	0	0	0
Vaporizer Voltage, V	3.86	3.80	3.79
Vaporizer Current, A	2.0	2.0	1.99
Vaporizer Heater Power, W	7.7	7.6	7.5
Neutralizer			
Keeper Voltage, V	20	22	21
Keeper Current, mA	370	370	370
Keeper Power, W	7.4	8.1	7.8
Heater Power, W	0	0	0
Vaporizer Voltage, V	1.10	0.80	0.6
Vaporizer Current, A	0.65	0.55	0.45
Vaporizer Heater Power, W	.7	.4	.3
Coupling Voltage, V	12.5	18	26
Output Beam Power, W	40	40	40.2
Total Input Power, W	78.3	78.6	78.6
Propellant Utilization Efficiency (including neutralizer), %	73	73	73
Electrical Efficiency, %	51	51	51
Over-all Efficiency, %	37.2	37.2	37.2
Discharge Loss, eV/ion	660	652	650
Thrust, mlb	0.46	0.46	0.46
Specific Impulse, sec	2920	2920	2920
Power-to-Thrust Ratio, W/mlb	170	171	171

T930

Beam deflection measurements were made 70 hours, 114 hours, and 162 hours of the thruster durability test. The data from first two sets were reduced and showed certain inconsistencies which have subsequently been resolved. Examination of thruster performance data revealed that the neutralizer-keeper voltage for these two sets was at least 20 V and in some cases higher. Since the Faraday cups of the beam scanner are provided with only -30 V bias to prevent electrons from entering the cups, it is believed that some of the neutralizer electrons may have penetrated this barrier to give erroneous readings. The third set of deflection data was taken with a high neutralizer flow rate to lower the neutralizer keeper voltage to 14 V. These results are shown in Table VIII and are in agreement with those obtained under Contract NAS 3-15385.² The results of Table VIII are shown graphically in Figs. 4 and 5. Deflections of $\pm 10^\circ$ are readily attained in the X and Y directions with accel currents remaining relatively constant at 0.08 mA. Because of the inconsistencies in the first two sets of data (attributed to energetic neutralizing electrons), the three sets of results could not be compared; however, the results of the third set demonstrate the capabilities of the SIT-5 deflection system.

Post-test inspection of the grids and neutralizer cathode showed no signs of wear. During disassembly of the thruster to inspect the main cathode, two of the four insulators which support the thruster flange and endplate were found to be fractured at the point where they are brazed to Kovar sleeves. These are the same type of insulators that fractured on SIT-5 (S/N 202) during the shake test and were noticed under the launch environment test results. Evidently these fractures occurred during the shake test of the S/N 201 module, but they were not detected until the locknuts on the insulator ends were loosened after the durability test was completed. These fractured insulators did not seem to affect the thruster durability tests. The insulators on S/N 201 module have since been replaced with redesigned supports that place all ceramic elements in compression rather than in tension.

TABLE VIII

Deflection Data for SIT-5 (S/N 201)

V_B Volts	V_{Ac} -Volts	I_B mA	I_{Ac} mA	V_x Volts	V_y Volts	θ_x Degrees	θ_y Degrees
1600	800	25	0.08	0	0	0	0
1600	800	25	0.08	300	0	5.9	0
1600	800	25	0.08	600	0	11.2	0
1600	800	25	0.075	-300	0	-5.5	0
1600	800	25	0.075	-600	0	-9.6	0
1600	800	25	0.080	0	300	0	5.9
1600	800	25	0.078	0	600	0	11.6
1600	800	25	0.075	0	-300	0	-5.6
1600	800	25	0.075	0	-600	0	-11.0

T931

TABLE IX

Set Point for Steady State Thruster Operation

Beam Voltage, $V_B = 1600$ V
Accel Voltage, $V_{Ac} = -800$ V
Discharge Voltage, $V_D = 45$ V
Beam Current, $I_B = 25$ mA
Main Cathode Heater Power, $P_{M, CH} = 0$ W
Neutralizer Cathode Heater Power, $P_{N, CH} = 0$ W

b. Performance Mapping

After completion of the Durability Test, a second neutralizer cathode and a burrette feed system was attached to the thruster, at the request of the NASA Project Manager. The cathode was located external to the ground screen and approximately 180° from the original neutralizer mounted within the ground screen shroud. This neutralizer was employed at all times when the performance mapping data was taken. The centerline of the aperture of the neutralizer keeper was 2.61 inches (6.62 cm) from the axis of the thruster. The face of the neutralizer keeper was parallel to the electrode system and located 1.64 inches (4.17 cm) from the downstream edges of the accel electrode. As shown in Fig. 19, these dimensions place the neutralizer keeper totally upstream of the cone that makes an angle of approximately 45° with the accel electrode. To ensure that steady state operation was fully established after this modification, the thruster was operated for 116 hours at the set point described in Table IX. After this period of set point operation, system parameters were varied from their nominal values to determine the effect on thruster performance.

Neutralizer-keeper current was varied to determine the effect on the neutralizer keeper voltage, thruster floating potential, and accelerator drain current. The results are plotted in Fig. 20. In all cases the accel drain current remained constant at 0.07 mA. The neutralizer-keeper voltage remained constant at 16 volts for neutralizer keeper currents greater than 360 mA, while the thruster floating potential* stayed within a 7 V to 9 V range. In its new location, the neutralizer coupled effectively with the ion beam, and thruster floating potentials were lower than those obtained from the previous neutralizer configurations. Similar results were obtained for neutralizer-cathode heater powers of 2.5 W and 5 W, respectively. Mercury flowrate to the

*The thruster floating potential is defined as the potential of the thruster ground screen with respect to the vacuum chamber walls. In the SIT-5 thruster system, this potential is identical with the neutralizer floating potential which is also identified in this report as the neutralizer coupling voltage together with the corresponding neutralizer coupling current.

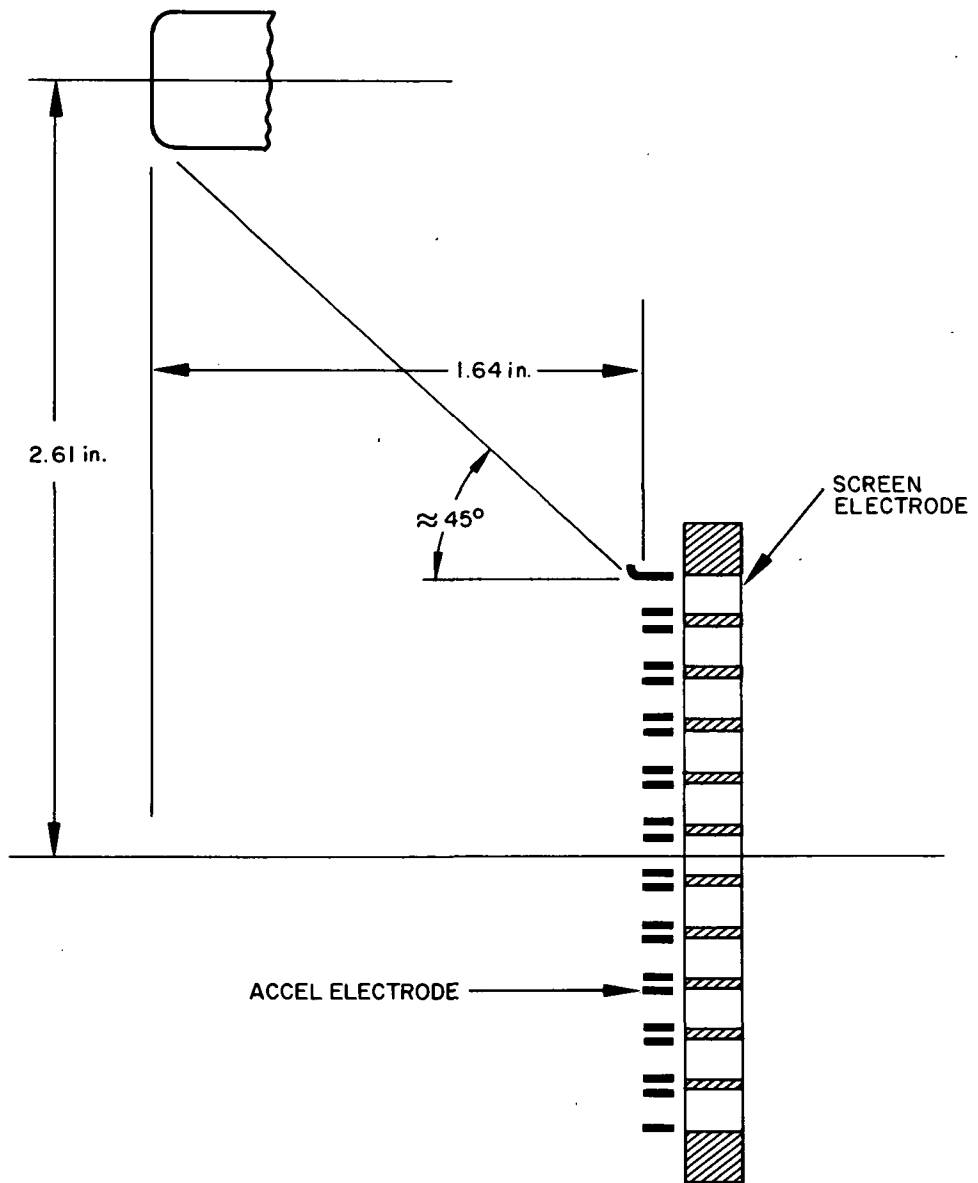


Fig. 19. Neutralizer position during performance mapping of S/N 201 Module (scale = 2x).

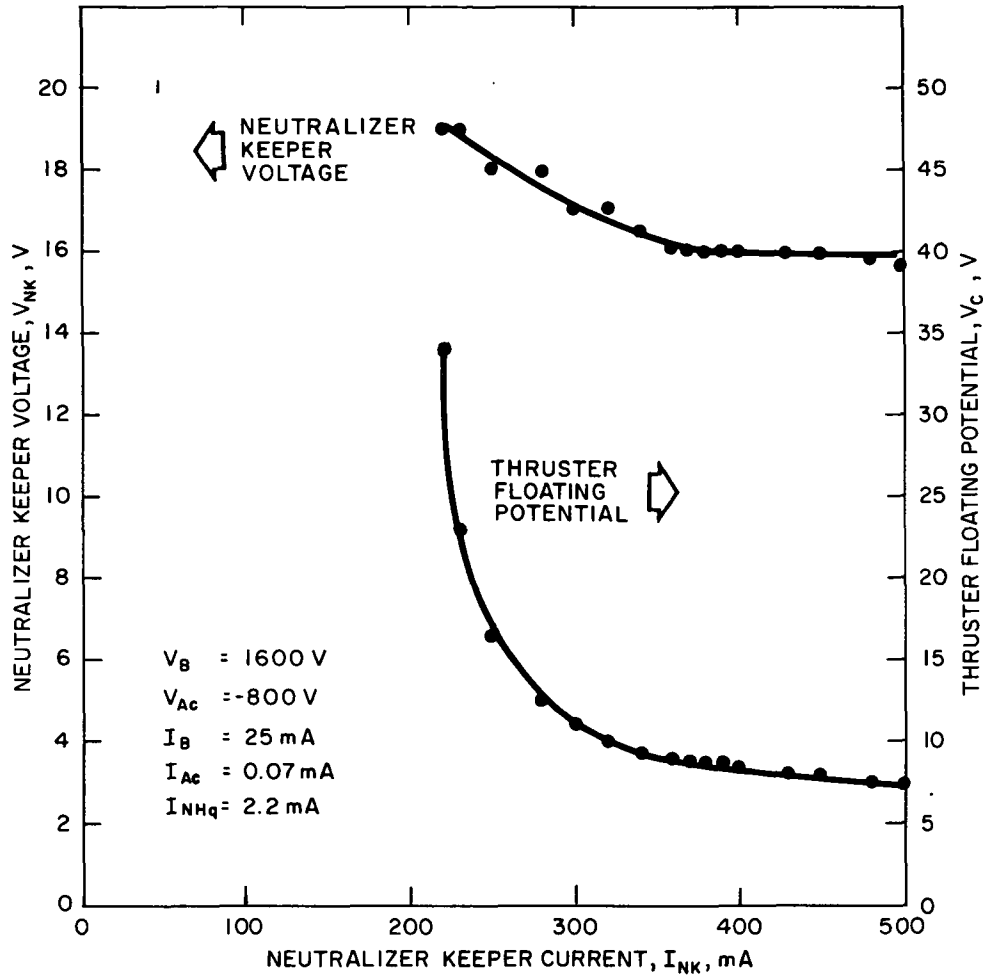


Fig. 20. Neutralizer-keeper current versus neutralizer-keeper voltage and neutralizer floating potential for neutralizer cathode heater = 0 W.

neutralizer cathode was varied to determine the effect on system performance. The neutralizer keeper voltage remained constant for flowrates of $I_{N, Hg} = 2$ to 3 mA while the thruster neutralizer floating potential rose from 8 to 14 V over the same range. Based on the data presented in Fig. 21, operation at the flowrate of approximately 2 mA appears to be a good choice since this is the point the keeper voltage starts rising and the neutralizing floating potential is about 8 V.

Main-keeper current was varied to determine the effect on the main-keeper voltage, discharge-chamber voltage, discharge-chamber current, and beam current. The results are plotted in Fig. 22. The main-keeper voltage reaches a maximum of 18 volts for main-keeper currents greater than 500 mA. The discharge-chamber current remains between 340 mA and 360 mA for all values of keeper current above 250 mA. The ion beam remains relatively constant at 25 mA until the keeper current is raised above the nominal operating value of 360 mA; this occurs because the discharge chamber voltage is decreasing at the same time. Data were also taken for a constant propellant flowrate and cathode-heater powers of 6.7 W, 13.3 W and 20 W with results very similar to those taken for zero power to the main cathode heater.

The effect of flowrate on discharge-chamber voltage, discharge-chamber current, and beam current was also determined. Measurements were made at flowrates 25% higher and 25% lower than this value by controlling the vaporizer temperature. These data are presented in Fig. 23. The discharge-chamber voltage varies from 60 V to 41 V, the discharge chamber current varies from 270 mA to 386 mA and the ion beam varies from 19 mA to 28.2 mA for that flowrate variation. It should be pointed out that these particular results are strongly dependent of the discharge-chamber power supply.

The effect of the net-accelerating voltage on the discharge-chamber voltage, discharge-chamber current, and accelerator-drain current was found for beams of 20, 25, and 30 mA, respectively. The beam and accel voltage which were used are shown in Table X.

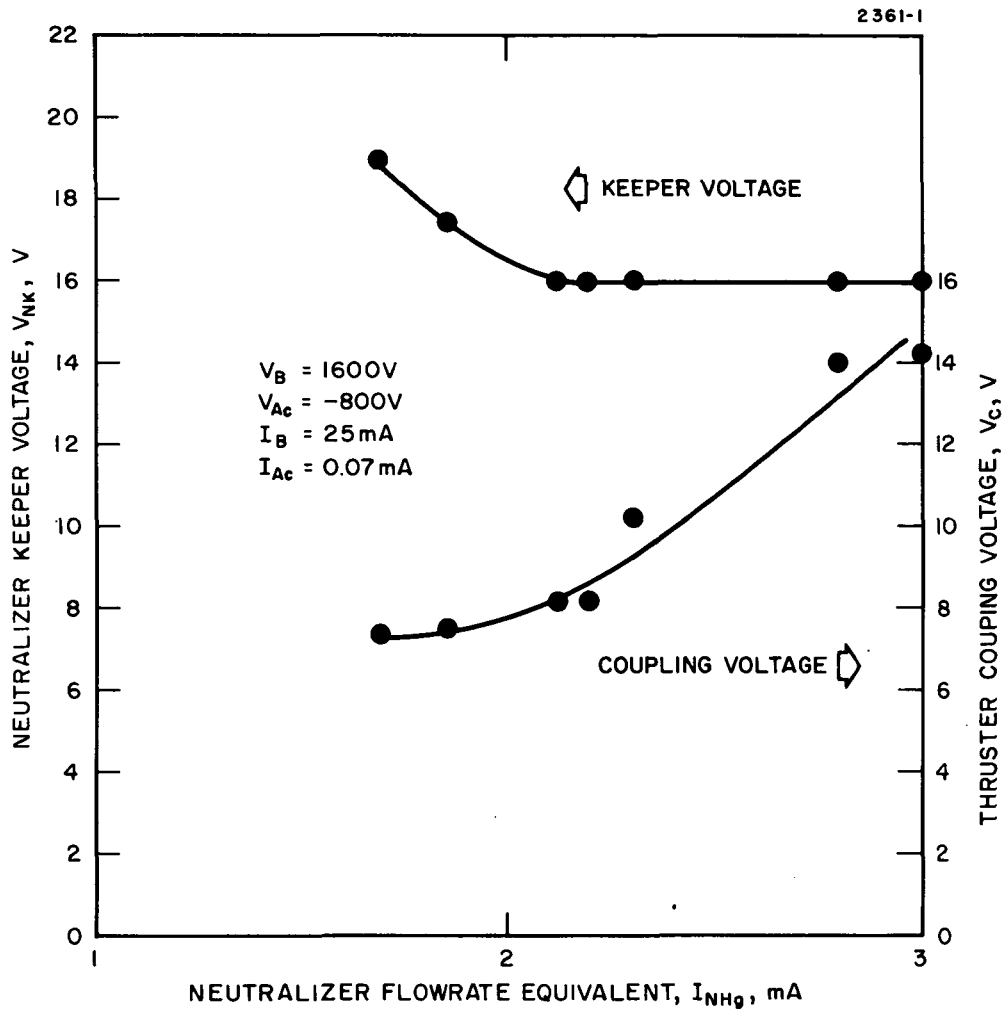


Fig. 21. Neutralizer flowrate equivalent versus neutralizer keeper voltage and neutralizer floating potential.

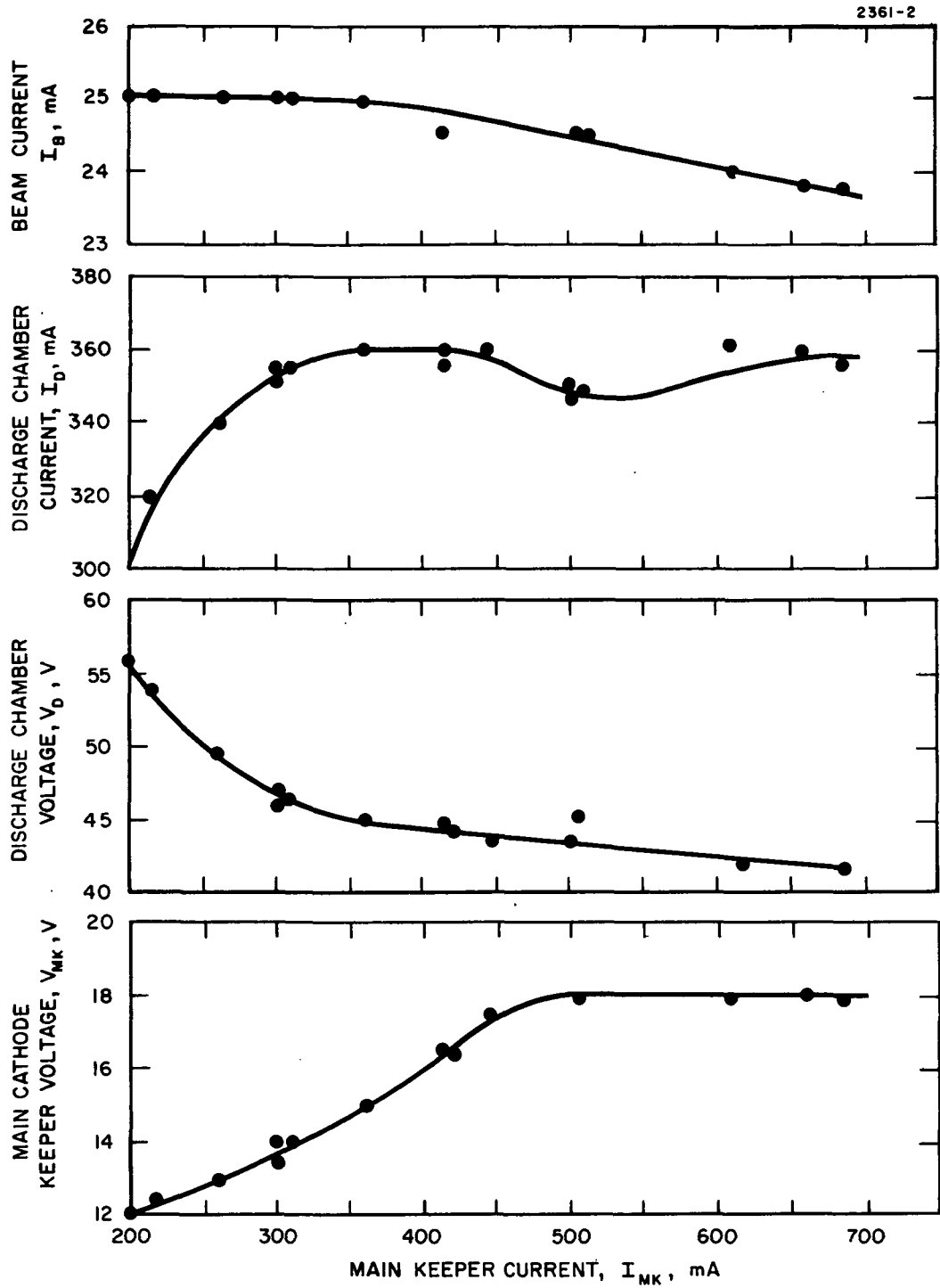


Fig. 22. Main keeper current versus main keeper voltage, discharge chamber voltage, discharge chamber current and beam current for constant flowrate and cathode heater power = 0 W.

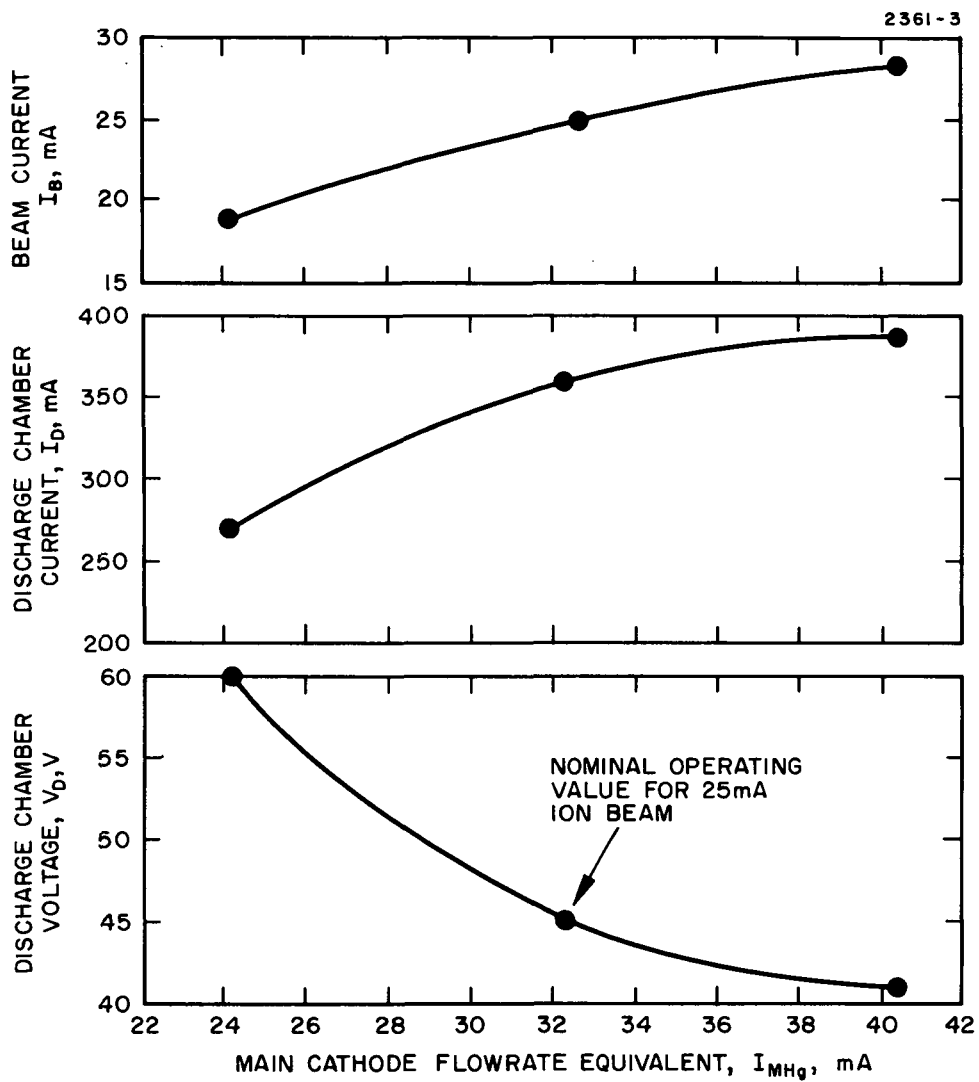


Fig. 23. Main cathode flowrate versus discharge chamber voltage, discharge chamber current and beam current for $V_B = 1600$ V and $V_{Ac} = -800$ V.

At each beam level the measured quantities remained relatively constant, although the discharge-chamber current and accel-drain current increased as the beam increased. Results of beam-current and accel-drain measurements are shown in Fig. 24. For the 25 mA ion beam, the nominal operating value is 2400 V ($V_B = 1600$, $V_{Ac} = -800$) which corresponds to a 0.07 mA accel-drain current. For this case the drain current remains constant down to 1800 V even though there is a slight drop in beam current at 2100 V. This curve shows that the nominal operating point for a 25 mA beam is approximately 400 V above the value where the beam current starts to drop. After the performance mapping was complete the thruster was weighed to determine the amount of mercury consumed by the main cathode. This value was used to calculate a utilization of approximately 70% including all startups. This compares favorably with the results of the Durability Test.

TABLE X

Beam and Accel Voltages for Net Accelerating Voltage Data

V_B (Volts)	V_{Ac} (-Volts)	$\left[V_B + \left -V_{Ac} \right \right]$ V_{Total} (Volts)
1200	900	2100
1300	900	2200
1400	900	2300
1600	900	2500
1600	800	2400

T 932

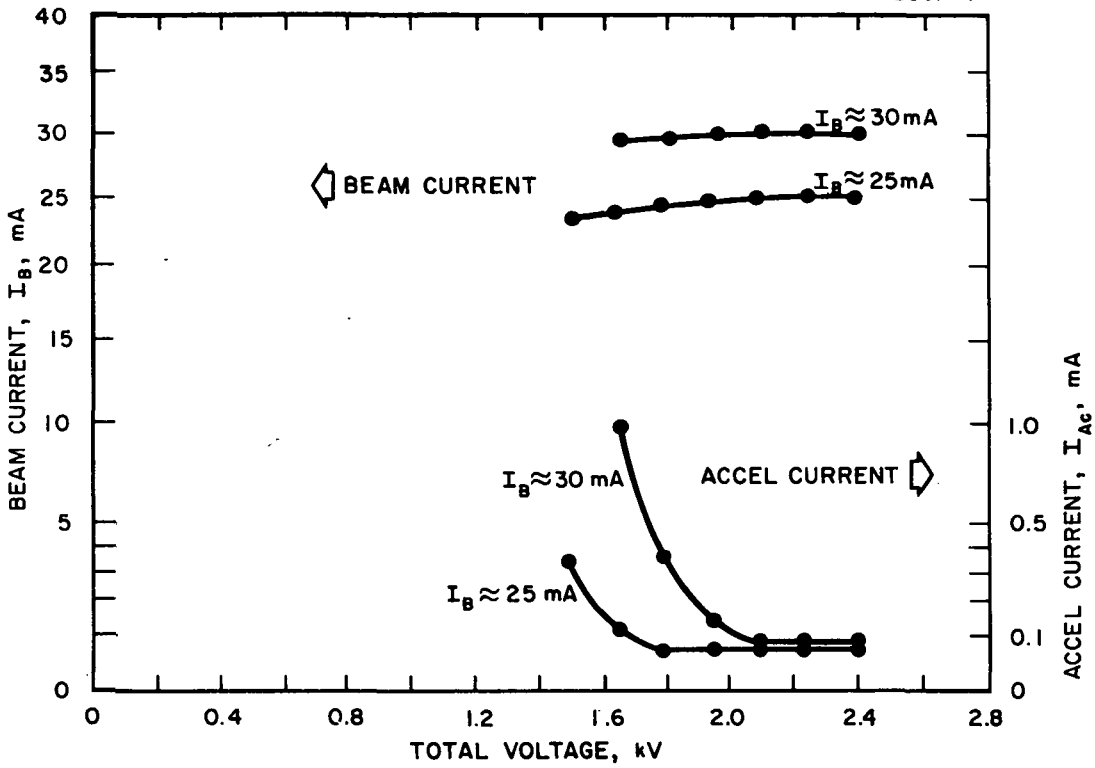


Fig. 24. Perveance curves for SIT-5 (S/N 201).

3. Cyclic Performance Tests

A complete module of the SIT-5 system was cycled from the power-off to the full beam on condition repetitively over various periods to establish its capability to function in the mode anticipated for north-south stationkeeping of a synchronous satellite. The duty cycle test was comprised of two parts. The first (≈ 400 hrs) approximated the cycling a thruster would experience in a north-south station keeping function, and the second (≈ 500 hrs) provided accelerated cycling to demonstrate the on-off capabilities of the system.

The Duty Cycle Test was performed in an oil-diffusion-pumped chamber approximately 4 feet in diameter and 12 feet long. The chamber has a cylindrical liquid-nitrogen cooled liner. The SIT-5 module was mounted to a chamber endplate and located on the axis of the chamber. A water cooled beam collector is at the opposite end of the chamber.

a. Four Hundred Hour Test (Long Cycles)

The schedule followed in this portion of the test was to approximate the cycles which the thruster would experience in a north-south station keeping function and to simulate the largest periods of eclipse the vehicle would experience. In a north-south station keeping function, the thruster operates on a less than 50% duty cycle; a beam on time of about 8 hours/day was used to simulate this. The neutralizer was ignited at all times except during the 72 minute simulation of vehicle eclipse (during periods of eclipse on a synchronous satellite, the thruster will be without power for a maximum of 72 minutes).

The 400 hour test was separated into three different cycle periods. The first 100 hour period was:

- Beam on 8 hours/day
- Neutralizer on 24 hours/day

The second 100 hour period was:

- Beam on 8 hours/day minus the time it required to discontinue power for 72 minutes and to restart the thruster.

- Neutralizer on 24 hours/day minus the time it required to discontinue all power for 72 minutes and to restart the neutralizer.

The final 200 hour period was:

- Beam on 8 hours/day
- Neutralizer on 24 hour/day minus the time it required to discontinue all power for 72 minutes and to restart the neutralizer.

A summary of the test is shown in Table XI. It can be seen that 18 cycles were made during the test. The last cycle was the shortest one since its end was determined by the completion of the 400 hour period. Cycles 1 to 4 comprise the first 100 hours. The first two days of operation experienced two neutralizer extinctions during the planned neutralizer-on period. This was attributed to the high chamber pressures which was created by turning off the flow of liquid nitrogen to the cryoliner. The liquid nitrogen was left on for the remaining 16 cycles with only one neutralizer extinction occurring on the 5th cycle. Cycles 5 through 8 comprise the second 100 hours of the test. These cycles went as planned except for the neutralizer extinction during the 5th cycle which was mentioned earlier. Cycles 9 through 18 were completed during the remaining 200 hours of this test. These cycles went according to the sequence outlined above.

Table XI also shows the startup time from the off condition to the neutralizer-on and beam-on condition. The first few cycles had longer starting times, because a conservative startup procedure was followed. As the test continued, this approach was changed and startup times ranged from 21 to 23 minutes. These shorter times followed the 72 minute all power-off condition. Thruster performance at the beginning, midway point, and end of the 400 hour test is shown in Table XII. The notable change that occurs between data sets is the increase in chamber discharge current that was necessary to maintain $V_D = 45$ V and $I_B = 25$ mA. This change started on the 15th cycle for no obvious reason, but is attributed to cathode-polepiece screen

TABLE XI

Summary of 400 Hour Test

Cycle No.	Date	Cycle Start Time	Beam on Time	Startup Time	Neutralizer on Time	Cycle Plan	Remarks
1	7/17/72	1019	6 hr 21 min	49 min	Minimum = 9 hr Maximum = 13 hr	Neutralizer on 24 hr; Beam on 8 hr	Liquid nitrogen turned off at end of day; Neutralizer went out during night
2	7/18/72	0945	8 hr	78 min	Minimum = 7 3/4 hr Maximum = 13 hr	Neutralizer on 24 hr; Beam on 8 Hr.	Liquid nitrogen turned off at end of day; Neutralizer went out during night.
3	7/19/72	0900	8 hr	38 min	24 hr	Neutralizer on 24 hr; Beam on 8 Hr	Liquid Nitrogen on to end of 400 hr test
4	7/20/72	0850	8 hr	29 min	24 hr	Neutralizer on 24 hr; Beam on 8 Hr	
5	7/21/72	0810	6 hr 52 min	36 min	Minimum = 8 hr Maximum = 13 hr	All power off 72 min. Neutralizer on 22 hr 48 min less start up time. Beam on 8 hr less start up time	First 72 min period with all power off. Neutralizer went out during night.
6	7/22/72	0941	7 hr 19 min	29 min	22 hr 19 min		
7	7/23/72	0933	8 hr 51 min	26 min	22 hr 23 min		
8	7/24/72	0945	7 hr	23 min	22 hr 25 min		
9	7/25/72	0835	8 hr	21 min	22 hr 34 min		
10	7/26/72	0833	8 hr	18 min	22 hr 34 min	All power off 72 min. Neutralizer on 22 hr 48 min less start up time. Beam on 8 hr.	
11	7/27/72	0835	8 hr	23 min	22 hr 13 min		
12	7/23/72	0845	8 hr	21 min	22 hr 35 min		
13	7/29/72	0833	8 hr	21 min	21 hr 32 min		
14	7/30/72	0735	8 hr	22 min	23 hr 31 min		
15	7/31/72	0834	8 hr	22 min	22 hr 34 min		
16	8/1/72	0835	8 hr	22 min	22 hr 33 min		
17	8/2/72	0835	8 hr	23 min	22 hr 32 min		
18	8/3/72	0841	16 min	23 min	40 min		Test concluded at the end of 400 hr.

TABLE XII

Thruster Performance During 400 Hr. Test

	1st Cycle Data	9th Cycle Data	17th Cycle Data
Beam Voltage, V_B , V	1600	1600	1600
Beam Current, I_B , mA	25	25	25
Accel Voltage, V_{Ac} , V	-800	-800	-800
Accel Current, V_{Ac} , mA	0.07	0.08	0.07
Discharge Chamber Voltage, V_D , V	45	45	45
Discharge Chamber Current, I_D , mA	323	330	430
Neutralizer Coupling Voltage, V_C , V	10.7	9.9	10.0
Neutralizer Coupling Current, I_C , mA	24.5	24.5	24.5
Main keeper Voltage, V_{MK} , V	15.6	14.8	13.8
Main keeper Current, $I_{M,K}$, mA	357	365	367
Neutralizer Keeper Voltage, $V_{N,K}$, V	16	14	14
Neutralizer Keeper Current, $I_{N,K}$, mA	359	365	368
Discharge Energy/ion, $V_{Disch.}$, eV/ion	582	594	774

T 935

erosion which is described below (see results of the post-test inspection). This change was quite abrupt, as can be seen in Fig. 25 which shows the chamber discharge current as a function of cycle number. Discharge current was increased manually to obtain a beam current of 25 mA. Since the accel current did not change during the test, it is assumed that the flowrate did not change appreciably.

b. Five Hundred Hour Test (Accelerated Cycles)

The second part of the Duty Cycle Test was an accelerated cycle test. The goal of this program was to accumulate 1000 duty cycles within 500 hours of accelerated test cycling. This test followed conclusion of the 400 hour test (without removing the thruster from the vacuum chamber) and was preceded by a short period of determining the timing of events for the accelerated cycle. A one-half hour cycle was set as a goal so that 1000 cycles could be completed within the 500 hour test period. The cycle chosen was a 10 minute off time, a 10 minute startup time, and a 10 minute neutralizer and beam-on time. Throughout the test, the cycle was completed in one half hour. The off time was always 10 minutes. Occasionally, the startup time took longer than 10 minutes and, if this were the case, the neutralizer and beam-on time was less than 10 minutes. Several adjustments were made early in the test, but a typical automatic startup sequence that was followed is shown in Table XIII. At the completion of a cycle, all power was turned off. (This event occurs at $t = 0$). At this time the main vaporizer and neutralizer vaporizer temperatures were 217°C and 174°C respectively.* The power remained off for 10 minutes during which time the main vaporizer temperature dropped to 100°C and the neutralizer vaporizer temperature dropped to 86°C . At the end of 10 minutes, approximately 2.3 A were supplied to each of the cathode heaters from constant current power supplies. Current was

* These temperature measurements are only approximate, because no temperature-controlled cold junction is maintained to reference thermocouple measurements.

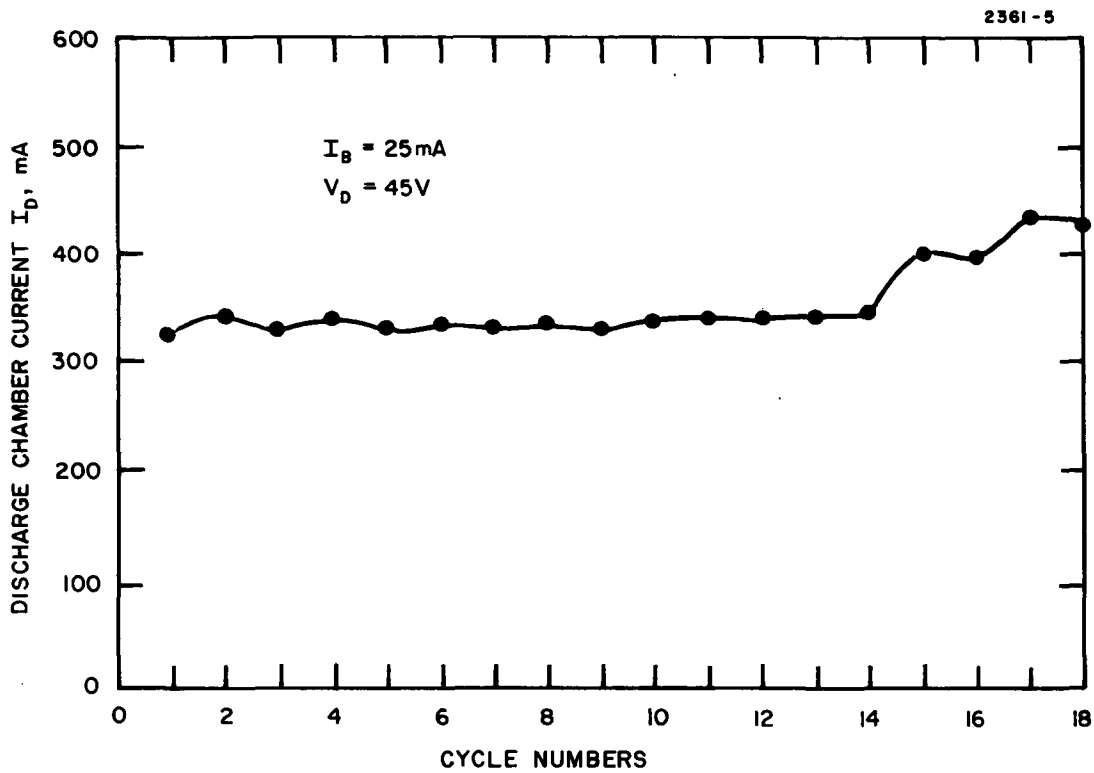


Fig. 25. Discharge chamber current as a function of cycle number.

also supplied to the vaporizer heaters at this time as shown in Table XIII. Fifteen minutes after the start of the cycle, the power values to the cathode heaters were increased while the power to the vaporizers remained the same. The discharge voltage was also turned on at this time. Five minutes later (20 minutes into the cycle), the neutralizer keeper voltage was turned up to 650 volts. If the neutralizer ignited, the main keeper voltage was turned on. Since the discharge voltage was on at this time, the main discharge came on as soon as the main keeper ignited. Usually, this happened instantaneously. Under no circumstances was the main-keeper voltage allowed to come on with the neutralizer off. The sequencer pulsed the keeper voltages if the keeper did not ignite; this timing sequence was 10 seconds on and 50 seconds off until the discharge commenced. As soon as the neutralizer started, a control loop regulated the power to the neutralizer vaporizer to achieve a neutralizer keeper voltage of about 13 V. The beam voltage and accel voltage suppliers were turned on one minute after both keepers and the main discharge were ignited; this event was defined as the neutralizer-on and beam-on condition. The neutralizer-on and beam-on condition continued until the end of the 30 minute cycle. A control loop on the main vaporizer was used to maintain a constant discharge-chamber voltage during this time. An automatic startup capability was programmed into the sequence to provide for the eventuality that either of the keepers went out.

The sequence described above was followed for 594 cycles of the accelerated cycle test. An eight channel recorder was used to monitor the following data:

- 1) Beam Current, I_B
- 2) Accel Current I_{Ac}
- 3) Main Cathode Heater Current, $I_{M, C}$
- 4) Neutralizer Cathode Heater Current, $I_{N, C}$
- 5) Neutralizer Keeper Current, $I_{N, K}$
- 6) Main Keeper Current, $I_{M, K}$

- 7) Neutralizer Vaporizer Heater Current, I_N, V
- 8) Discharge Chamber Voltage = V_D

Figure 26 shows the results of eleven such cycles as recorded on the chart paper used throughout the test.

The major change made during this test period was the adjustment of discharge chamber current and voltage. The requirement of increasing the discharge chamber current to maintain a 25 mA beam, that began in the 400 hour test, continued into the accelerated cycle test. At the start of the accelerated cycle test, a discharge chamber current of 450 mA and a discharge voltage of 45 volts was used to obtain a 25 mA beam. During the second day of the test, the discharge chamber current was raised to 500 mA to obtain a 22 mA beam with a 45 V discharge chamber current. On the 8th day of the test the discharge chamber voltage was dropped to 40 volts and the discharge chamber current was decreased to 400 mA at the direction of the NASA Project Manager. This selection of discharge-chamber parameters provided only 16.5 mA beam, but was based on parameter values being used at the time in Lewis Research Center life test of a SIT-5 thruster and producing 25 mA beam under normal circumstances. These values were maintained to the end of the 594th cycle.

After 594 cycles of the accelerated cycle test, an open circuit developed in the main vaporizer heater which required that the sequence be changed. The neutralizer continued to cycle for 1009 cycles and the main cathode heater also cycled for 1009 cycles, but the beam-on condition could not be maintained after the 594th cycle. The modified cycle that was followed after the loss of the main vaporizer heater is shown in Table XIV. The neutralizer startup sequence was the same as before. The main cathode tip heater was maintained at the high heat level for the remaining part of the cycle since the main keeper would not ignite. This was because the loss of the main vaporizer heater prevented an adequate mercury flowrate in the main vaporizer. This modified cycle continued until the end of the accelerated cycle test. The actual elapsed time of the test was 527 hours.

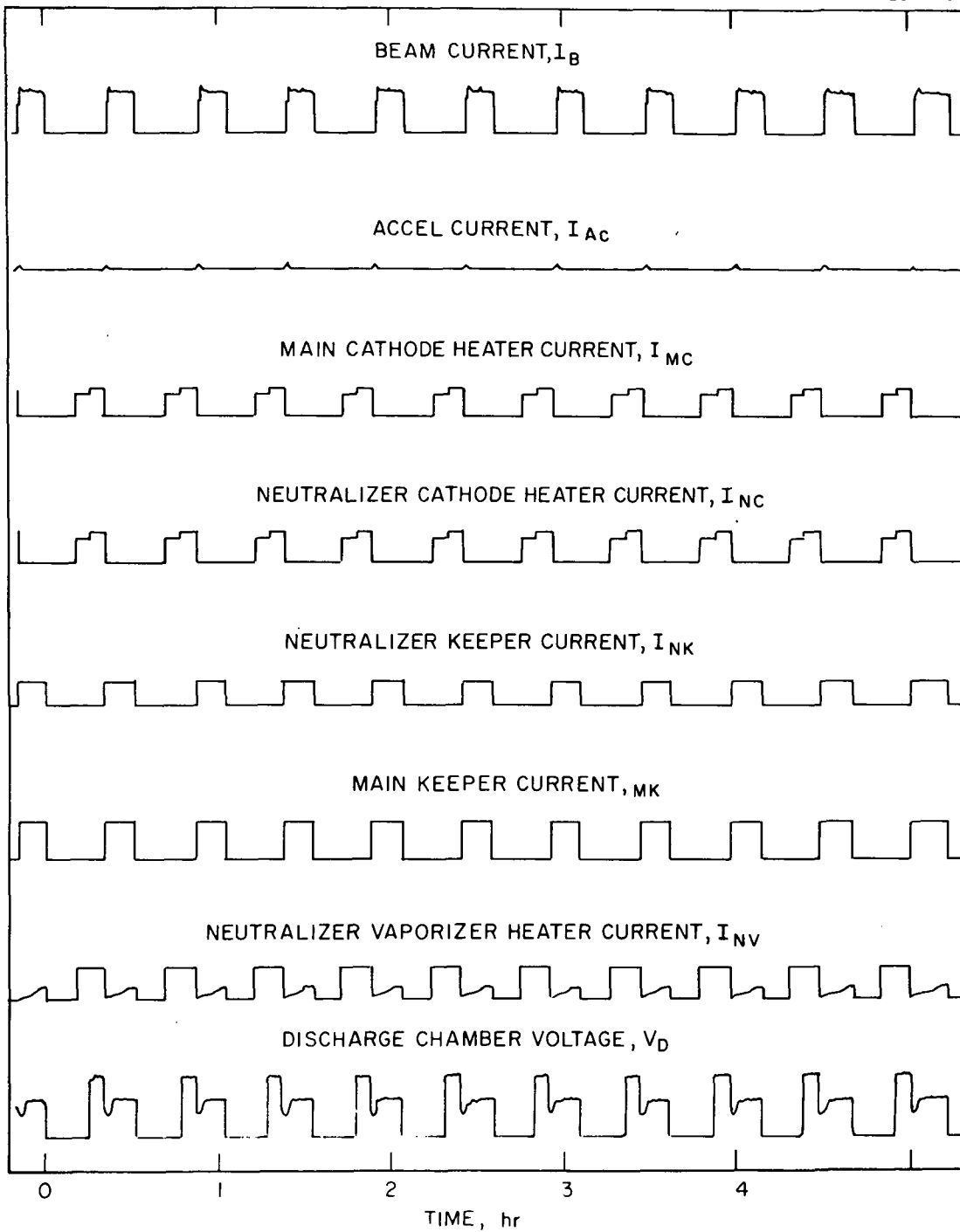


Fig. 26. Eight channel recorder data for accelerated cycle test.

Early in the test, there were a few interruptions in the cycle to change the sequence or timing of events. This necessitated greater than 500 hours to accumulate 1000 cycles. The neutralizer went through 1009 cycles, the beam-on went through 594 cycles, and the main cathode heater experienced 1009 cycles. The number of cycles given are only those accumulated during the accelerated cycle test. Approximately 30 additional cycles were accumulated prior to the start of the accelerated cycle test.

c. Post-Test Inspection

At the end of the accelerated cycle test, the thruster was removed from the vacuum chamber and taken apart. The electrodes showed only minor wear. This was expected since the beam-on time was only about 250 hours for the entire duty cycle test. After the electrodes, shell, and anode were removed, the 0.001 in. nickel wire mesh which had been used to screen the ports of the cathode polepiece was found to be eroded away completely. This observation explained the reason it was necessary to keep increasing the discharge chamber current; as the material eroded away more discharge current was needed to compensate for the loss of electrons through the holes in the cathode polepiece.

It is believed that high discharge-chamber erosion was initiated by the high discharge voltage ($V_D > 65V$), which obtained when the beam voltage was first turned on, but before the vaporizer-heater regulator could affect control over the mercury flow in the main vaporizer. This was corrected eventually by leaving the vaporizer control loop open until after the beam and accel voltages were turned on. In this mode, high voltage was applied without difficulty under a rich-feed condition in which the discharge voltage was only 30 V at high-voltage turn on. Although this sequence change was made during the second day of the accelerated cycle test, the damage to the nickel mesh had already been done. To minimize the problem in the future, it is suggested that the sputter resistance of the inner screen material should be increased by changing to a heavier gauge tantalum mesh such as that employed for SIT-5 testing at LeRC. ⁶

A photograph of the baffle and the baffle support is shown in Fig. 27. It can be seen that the part of the threaded rod above the nut is tapered from erosion. This observation amplifies a concern over operation at high discharge-chamber voltage.

After conclusion of the Duty Cycle Test, the main vaporizer heater was removed from the vaporizer and examined to determine the cause of the open circuit which developed after 594 cycles. A photograph of the main vaporizer heater defect that created the open circuit is shown in Fig. 28. The central conductor is still intact, but the outer sheath (which is used as the current return) is severed and was what created the open circuit. A thin spot in this sheath could have been created during the swagging process used in the production of the heater. Passing higher than normal currents through this thin material could have caused it to develop a hot spot which, in turn, vaporized the material. This was the first time a vaporizer heater had become defective during testing of a SIT-5 thruster. At the start of the duty cycle test, it had been noted that the main vaporizer heater required more power than had similar heaters on other SIT-5 thrusters. This difference was attributed to poor thermal contact between the main vaporizer body and the outer sheath of the heater. Operation under these conditions served to overstress the heater, because the heater element itself was operated at a temperature ($\sim 900^{\circ}\text{C}$) which was far above the normal value. To prevent this from happening again, it is suggested that for future fabrications the heater should be brazed to the vaporizer body to improve the transfer of heat to the vaporizer.

E. AREAS FOR CONTINUED DEVELOPMENT

The SIT-5 thruster was operated with the beam-deflection system only after it was combined with its flight-type propellant feed system. In this configuration, electrical performance was virtually unchanged, and no significant change in propellant-utilization efficiency was detectable from mass measurements conducted before and after

M8966

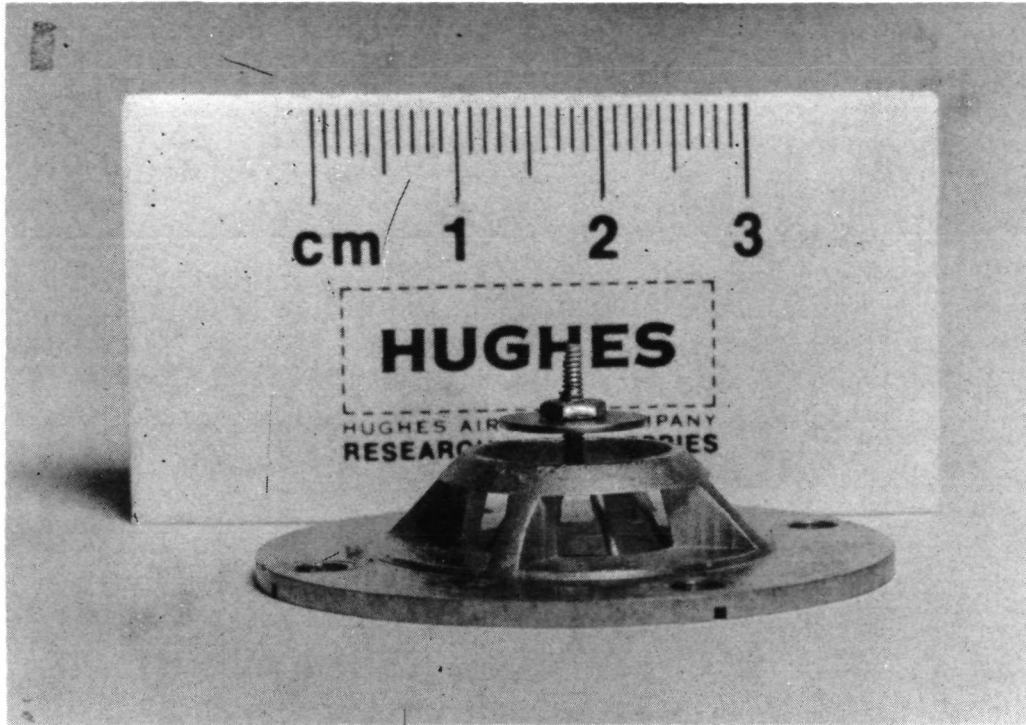


Fig. 27. Baffle and baffle support after duty cycle test.

M8967



Fig. 28. Main vaporizer heater defect.

that operation under the subject contract effort. During operation of the complete thruster system under NASA Contract NAS 3-15385, however, propellant measurements were carried out with a burrette feed system, and a significant decrease in propellant utilization was reported.² This discrepancy has not been resolved under the subject effort, and the need for further study is indicated.

Reduction in discharge voltage to a level $V_D \lesssim 40$ V is also recommended for future operation of the SIT-5 thruster to reduce the rate of discharge-chamber erosion due to ion bombardment of cathode-potential surfaces. Since test conducted at HRL were not of sufficient duration to observe significant wear,* this recommendation is based on theoretical considerations¹³ and on SIT-5 operating experience obtained by LeRC.^{17, 18, 19}

*The only case of significant discharge - chamber erosion was observed after completion of the Duty Cycle Test. These observations cannot be related to normal discharge erosion rates, however, because of extended periods of operation at $V_D > 65$ V during the early part of the test.

Page Intentionally Left Blank

SECTION III

SUMMARY OF RESULTS

Under the subject program, the SIT-5 propulsion system has advanced from a predesign concept to a performance qualified prototype device. Dynamic analysis and vibration testing have confirmed the structural integrity of the system design. The thruster shown in Fig. 2 has been qualified for shock (30 G), sinusoidal (9 G), and random (19.9 G rms) vibrations which establishes the system's capability to survive booster launch. Performance testing with a conventional beam-extraction system has demonstrated operation at specific impulse $I_{sp} = 3040$ sec with total efficiency $\eta_T = 43\%$. Similar performance with a high-angle (10 degrees) electrostatic beam-deflection system demonstrates the thruster's capability for attitude control and stationkeeping of synchronous satellites.

Page Intentionally Left Blank

REFERENCES

1. J. Hyman, Jr., "Design and Development of a Small Structurally Integrated Ion Thruster System," Final Report NAS 3-14129, NASA CR 120821, Hughes Research Laboratories, Malibu, California, Oct. 1971.
2. H.J. King, *et al.*, "Thrust Vectoring Systems," Final Report NASA Contract NAS3-15385, NASA CR-121142, Hughes Research Laboratories, Malibu, California 90265, December 1972.
3. W.R. Kerslake, D.C. Byers, and J.F. Staggs, "SERT II Experimental Thruster System," AIAA Paper 67-700 (1967).
and
D.C. Byers and J.F. Staggs, "SERT II Flight-Type Thruster System Performance," AIAA Paper 69-235 (1969).
4. D.F. Hall, R.F. Kemp, and H. Shelton, "Mercury Discharge Devices and Technology," AIAA Paper 67-669, AIAA Electric Propulsion and Plasma Dynamics Conference, Colorado Springs, Colorado, September 11-13, 1967.
5. S. Nakanishi, W.C. Latham, B.A. Banks, and A.J. Weigand, "Status of a Five-Centimeter-Diameter Ion Thruster Technology Program," AIAA Paper 71-690, AIAA/SAE 7th Propulsion Joint Specialists Conference, Salt Lake City, Utah, June 14-18, 1971.
6. A.J. Weigand, "5-Cm Diameter Ion Thruster Development Program Summary, June 1972," NASA TMX-68110, Lewis Research Center, Cleveland, Ohio, July 1972.
7. S. Nakanishi, "Durability of a Five-Centimeter Diameter Ion Thruster System," AIAA Paper 72-1151 (1972), AIAA/SAE 8th Joint Propulsion Specialists Conference, New Orleans, Louisiana (Nov. 29-Dec. 1, 1972).
8. H.J. King, C.R. Collett, and D.E. Schnellker, "Thrust Vectoring System, Part I, 5 cm Systems," NASA CR-72877, Hughes Research Laboratories, Malibu, California, June 1971.
9. T.D. Masek and E. V. Pawlik, "Hollow Cathode Operation in the SE-20C Thruster," Space Program Summary 37-53, Vol. III, Jet Propulsion Laboratory, Pasadena, California, October 1968.
and
T.D. Masek and E.V. Pawlik, "Thrust System Technology for Solar Electric Propulsion," AIAA Paper 68-541, AIAA 4th Electric Propulsion Joint Specialists Conference, Cleveland, Ohio, June 10-14, 1968.

10. J. Hyman, Jr., et al., "High-Temperature LM Cathode Ion Thruster," Final Report NASA Contract JPL 952131, Hughes Research Laboratories, Malibu, California 90265, April 1969.
11. W. Knauer, "Power Efficiency Limits of Kaufman Thruster Discharge," AIAA Paper 70-117, AIAA 8th Aerospace Sciences Meeting, New York, New York, January 19-21, 1970.
12. J. Hyman, Jr., et al., "Development of a Liquid-Mercury Cathode Thruster System," *J. Spacecraft and Rockets* 8, 707 (1971).
13. R.V. Stuart and G.K. Wehner, "Sputtering Yields at Very Low Bombarding Energies," *J. Appl. Phys.* 33, 2345 (1962).
14. H.H. Cooley, "SIT-5 Thruster Loads Document," HAC Report No. 4112.22.118, August 1971.
15. J.K. Lippitt and J.S. Quiaoit, "Ion Thruster Engine SIT-5 Preliminary Loads Report," NAC Report No. 4112.24.52, September 1971.
16. P.P. Bijlaard, "Stresses in Pressure Vessels," Welding Research Supplement, December 1955.
17. S. Nakanishi, and R.C. Finke, "A 2000-Hour Durability Test of a 5-Centimeter Diameter Mercury Bombardment Ion Thruster;" NASA TM X-68155 (1972).
18. John L. Power, "Sputter Erosion and Deposition in the Discharge Chamber of a Small Mercury Ion Thruster," Proposed Paper, AIAA Lake Tahoe, October-November, 1973.
19. S. Nakanishi and R.C. Finke, "A 9700-Hour Durability Test of a Five Centimeter Diameter Ion Thruster," Proposed Paper, AIAA Lake Tahoe October-November, 1973.